Standardized Photometric Calibrations for Panchromatic SSA Sensors

Philip J. Castro[1], Tamara E. Payne[1], Adam M. Battle[1], Zachery W. Cole[1], Joseph W. Moody[2], Stephen A. Gregory[1], Phan D. Dao[3]

[1] Applied Optimization

714 East Monument Ave, Suite 204

Dayton, OH 45402

[2]Brigham Young University

Department of Physics and Astronomy

Provo, UT 84602

[3]AFRL/RVBY

3550 Aberdeen Ave. SE

Kirtland AFB, NM 87117-5776

ABSTRACT

Panchromatic sensors used for Space Situational Awareness (SSA) have no standardized method for transforming the net flux detected by a CCD without a spectral filter into an exo-atmospheric magnitude in a standard magnitude system. Each SSA data provider appears to have their own method for computing the visual magnitude based on panchromatic brightness making cross-comparisons impossible. We provide a procedure in order to standardize the calibration of panchromatic sensors for the purposes of SSA. A technique based on theoretical modeling is presented that derives standard panchromatic magnitudes from the Johnson-Cousins photometric system defined by Arlo Landolt. We verify this technique using observations of Landolt standard stars and a Vega-like star to determine empirical panchromatic magnitudes and compare these to synthetically derived panchromatic magnitudes. We also investigate color terms caused by differences in the quantum efficiency (QE) between the Landolt standard system and panchromatic systems. We evaluate calibrated panchromatic satellite photometry by observing several GEO satellites and standard stars using three different sensors. We explore the effect of satellite color terms by comparing the satellite signatures. In order to remove other variables affecting the satellite photometry, two of the sensors are at the same site using different CCDs. The third sensor is geographically separate from the first two allowing for a definitive test of calibrated panchromatic satellite photometry.

1. INTRODUCTION

The Johnson photometric system is a set of filters in the optical wavelength region; the UBV spectral regions were established by [1], and [2] later added the RI spectral regions [3]. An additional RI system was also defined by [4], and [5] later modified this RI system [6]. The final definition of the Johnson-Cousins standard system ($UBVR_CI_C$) is the result of extensive work by Arlo Landolt [7]. He published a list of standard stars in the UBV system and [6] extended this list to include stars in the Cousins R and I bands. Most astronomers use Landolt standard stars to transform their system to that of the Johnson-Cousins system [8]. The Johnson photometric system has been used by the astronomical community for decades [7] [6] [9] [10] [11]. For a more thorough discussion of the development and evolution of the Johnson system see [6] and [3]. This photometric system has historically been used for filter observations of satellites [12] [13]. The calibration of satellite observations using the Johnson photometric system requires calibration stars in the same system – i.e. secondary standard stars that have been observed via the same filters and whose relationship to primary standard stars has been well established. Recent calibration star catalogs include Landolt standard stars [10] [11], as well as secondary standards from Stetson [14] and near secondary standards from Henden [8].

For greater sensitivity and sensor simplicity, many Electro-Optical (EO) sensors used to collect visible measurements of Resident Space Objects (RSOs), i.e. satellites and debris, do not have spectral filters in their optical path. Furthermore, the Space Situational Awareness (SSA) scientific community does not have a calibrated panchromatic (Open)[1] system analog to the photometric standard systems of Johnson-Cousins or Sloan. Thus, instrumental magnitudes are transformed to a pseudo-standard magnitude that has removed the atmospheric effects and put the magnitudes on some relative scale, but not on a standard scale such that photometry from different sensor systems are comparable. With the advances in service-oriented architectures, multi-site, multi-sensor data fusion is a reality; but the calibrations of panchromatic photometry lag behind. The purpose of this work is to lay the scientific foundation for a standardized process to transform panchromatic brightness measurements to a standard system for the SSA community as a whole.

2. PANCHROMATIC CALIBRATION PROCEDURE: THEORETICAL MODELING

We perform theoretical modeling in order to calculate the Open magnitude of a standard star from [10]. We anchor this synthetically derived Open magnitude to the Johnson-Cousins photometric system by using the UBVRI catalog values from [10]. First we calculate the synthetic instrumental flux of the UBVRI bands for a star. We do this by convolving the stars spectrum with the transmission of the filter curves and the quantum efficiency (QE) [9]. This results in synthetic instrumental fluxes for the UBVRI bands that by themselves are arbitrarily scaled, but the relative synthetic instrumental fluxes between the UBVRI bands is accurate. To put these arbitrary synthetic instrumental fluxes on a system, we calculate the measured instrumental flux of the UBVRI bands as observed by Landolt's system for this star. The measured instrumental flux is what provides an anchor that will eventually place the synthetic instrumental flux onto the Johnson-Cousins system. We perform a chi-squared like best fit between the synthetic instrumental fluxes and the measured instrumental fluxes for the BVRI bands, where the minimum chi-squared determines the scaling factor. The scaling factor for a best fit between the synthetic instrumental fluxes and the measured instrumental fluxes is applied to the normalized spectrum, calibrating the spectrum and simulating as if the star were observed by Landolt's system. The panchromatic synthetic instrumental flux of the star is then calculated, and likewise, the panchromatic synthetic instrumental flux of Vega is calculated using the flux calibrated

[1] Panchromatic refers to all visible wavelengths incident on the CCD sensor or other light collecting device. It is used interchangeably with "clear" to denote the use of a clear filter that passes all the visible light through and "open" to denote no filter present in the optical path.

spectrum of Vega. This results in a calibrated Open magnitude of the star on the Johnson-Cousins photometric system. We repeat this pipeline for each star in our standard star catalog.

2.1 Creation of Catalog

The photometric star catalog from [10] (in their Table 2) was acquired from VizieR[2]. This catalog was cleaned for standard stars by applying the following criteria to each star:

1. Number of observations greater than 4
2. Number of nights observed greater than 1
3. Mean error of the mean of V, B-V, U-B, V-R, R-I, and V-I photometry was less than 0.02.

This resulted in a star catalog containing photometry (V, B-V, U-B, V-R, R-I, and V-I) for 354 stars (out of 595) that we now consider to be 'standard stars'.

The spectral type catalog from [15] (in their Table 7) was acquired from VizieR. This catalog contained all of the stars from [10] (except for one star), with spectral types derived from spectral fitting to the measured photometry. The 141 spectra used for spectral fitting include Vega, 131 library spectra from Pickles Spectral Library [16], eight CALSPEC spectra, and one DA1/K4V double-star spectrum. The quality of the fit of the spectra to the photometry is given by a fitted rank, with 1 being the best [15]. See [15] for more details. This catalog was cleaned for the type of fitted spectral type and for the quality of the fitted spectral types. Spectral types of white dwarfs and Vega were removed, since we will only be using Pickles Spectral Library [16] in this paper. We removed any star with a fitted rank > 1, in order to use only the fitted spectral types of the best quality. The M dwarf spectral types that were given to one-tenth of a subtype (M4.2V, for example) were rounded to the nearest subtype (M4V, for example). This resulted in a catalog from [15] of 487 stars.

The cleaned catalog of [10] and the cleaned catalog of [15] were then cross-correlated to assign a spectral type to the standard stars of [10]. The stars from our cleaned catalog of [10] without a spectral type from the cleaned catalog of [15] were removed. This provided a catalog of 289 standard stars from [10] with spectral types. This provides the necessary input for each star, photometry and spectral type, to perform modeling to calculate the open magnitude.

2.2 Calculating Synthetic Instrumental Fluxes

The QE curve of the RCA 31034A photomultiplier serial No. N49701 from [9] was retrieved from Vizier, this is shown in Fig. 1. There were several photomultipliers used in [9] and [10], RCA and Hamamatsu photomultipliers in [9], and RCA, Hamamatsu, and LSU (a successor to an RCA model) photomultipliers in [10]. The QE of the Hamamatsu photomultiplier was not published. However, [10] provides evidence to indicate that the RCA and Hamamatsu photomultipliers are quite similar. We use the RCA 31034A photomultiplier serial No. N49701 QE curve to be representative of the QE of Landolt's system defining the Johnson-Cousins photometric system. We regard the QE of the detector to also be representative of the telescope throughput (not including the filters). The QE was truncated at 3000 Angstroms to provide an effective atmospheric cutoff. The transmission curves of the UBVRI

[2] http://vizier.u-strasbg.fr/
"VizieR provides access to the most complete library of published astronomical catalogues and data tables available on line organized in a self-documented database. Query tools allow the user to select relevant data tables and to extract and format records matching given criteria."
[A&AS 143, 23 (2000)]

filters from [9], used in [9] and [10], CTIO's filter set No. 3, were retrieved from Vizier and are shown in Fig. 2. The QE and filter transmission curves are needed for theoretical modeling of the Johnson-Cousins photometric system.

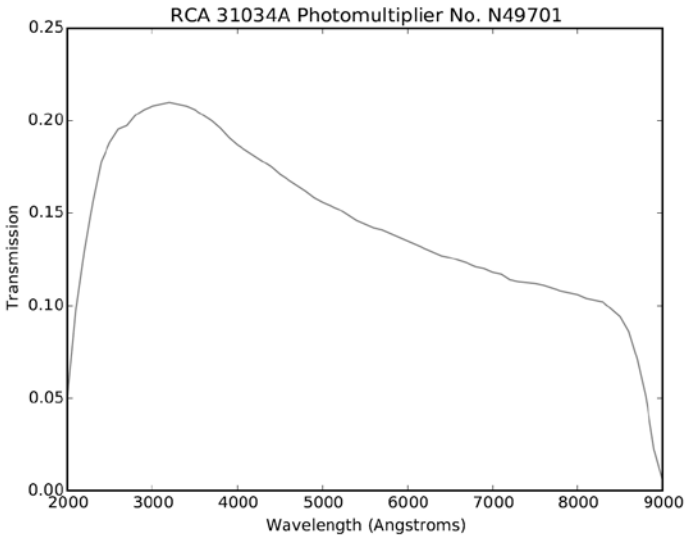

Fig. 1. Typical QE transmission defining the Johnson-Cousins photometric system.

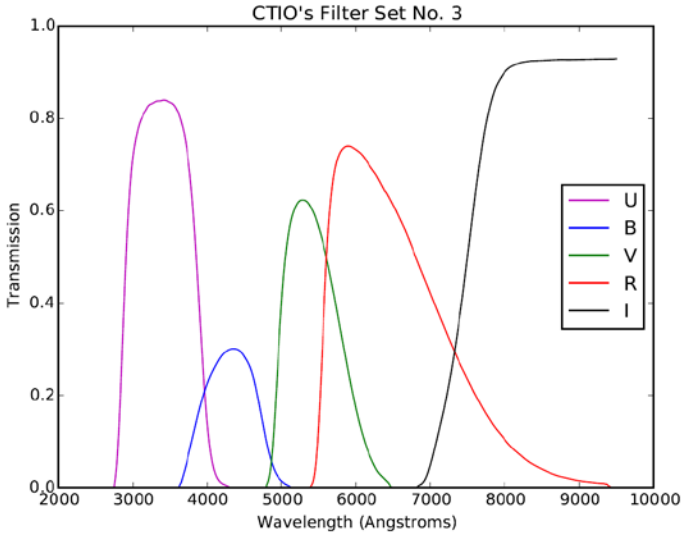

Fig. 2. Filter transmission curves for the UBVRI filters defining the Johnson-Cousins photometric system.

We retrieved 131 spectra from Pickles Spectral Library[3,4] [16]. We retrieved the 1150-10620 Angstrom library UVILIB since we are only concerned with optical wavelengths. The library contains spectral types from O5V to

[3] For more details of the library see, http://www.stsci.edu/hst/observatory/crds/pickles_atlas.html

[4] The ftp site where the library was retrieved can be found at, ftp://ftp.stsci.edu/cdbs/grid/pickles/dat_uvi/

M2I, including all luminosity classes (V, IV, III, II, and I). However, it does not contain a complete grid of spectral types, for example, for GV spectra it contains G0V, G2V, G5V, and G8V. The library also contains spectral types with 'weak' or 'rich' metallicity with respect to solar. It is important to note that the spectra from Pickles Spectral Library are exo-atmospheric. They already have the effects of the Earth's atmosphere removed.

Photomultiplier tubes like CCD's are photon-counting devices. The units of flux that appears in the Pogson equation are photons s^{-1} cm^{-2}. To convert between a spectrum whose flux is in energy units to a spectrum whose flux is in photon units it is necessary to divide the flux in energy units by hν, the energy per photon (E_{photon}= hν) [17]. Using c = λ ν, we get E_{photon} = hc/λ. Therefore we convert the spectrum whose flux is in energy units by multiplying by λ/(hc). The wavelength term in the multiplication makes the spectrum shape become redder. We use the conversion for photon energy associated with wavelength λ from [18] to convert the spectra from Pickles Spectral Library from units of ergs s^{-1} cm^{-2} $Angstrom^{-1}$ to photons s^{-1} cm^{-2} $Angstrom^{-1}$. A normalized G2V spectrum from Pickles Spectral Library is shown in Fig. 3.

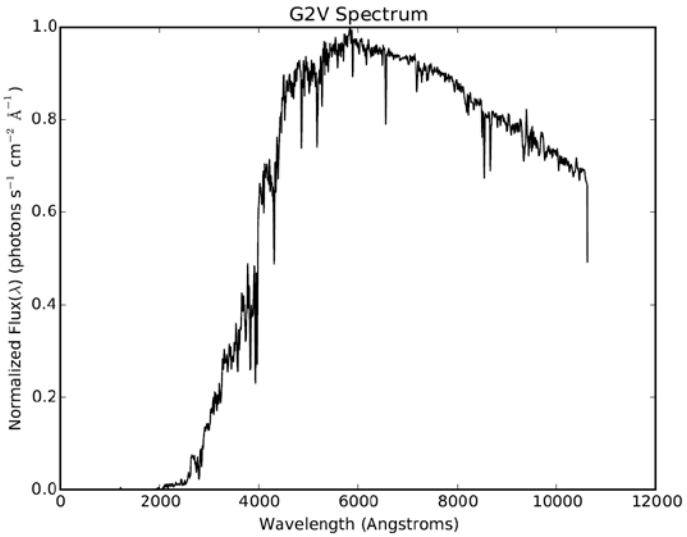

Fig. 3. Normalized G2V spectrum from Pickles Spectral Library [16].

We calculate the synthetic instrumental fluxes to simulate what Landolt's system would measure if observing a star with a particular spectral type. To calculate the synthetic instrumental fluxes we performed theoretical modeling using the Pickles Spectral Library, and the QE and filter curves from [9]. This is accomplished by taking convolutions of flux with transmission curves to simulate the flux that would reach the detector as a function of wavelength. In convolving two curves we first put the higher resolution curve onto the wavelength grid of the lower resolution curve via linear interpolation. The QE [9] has the lowest resolution at 100 Angstroms.

Fig. 4 below shows this process visually for a G2V spectrum (SA109-537 has a spectral type of G2V). We convolve the spectrum with the transmissions in the order that they occur when observing, first the light from the star passes through the filter (UBVRI) and then interacts with the detector (QE). We convolve the spectrum of the star (black solid line) with the U band transmission (magenta dashed line). Then we convolve the convolution of the spectrum and the U band transmission (magenta dotted line) with the QE (gray solid line). The resulting convolution is shown

at the bottom (magenta solid line). This process is repeated for the B (blue lines), V (green lines), R (red lines), and I (black lines excluding the spectrum) bands. We integrate the area under the curve to calculate the synthetic instrumental flux for each band. The synthetic instrumental flux value is arbitrary since we do not have a flux calibrated spectrum for the star and we used a normalized spectrum. The important characteristic is that the relative synthetic instrumental flux of one band to the other is accurate.

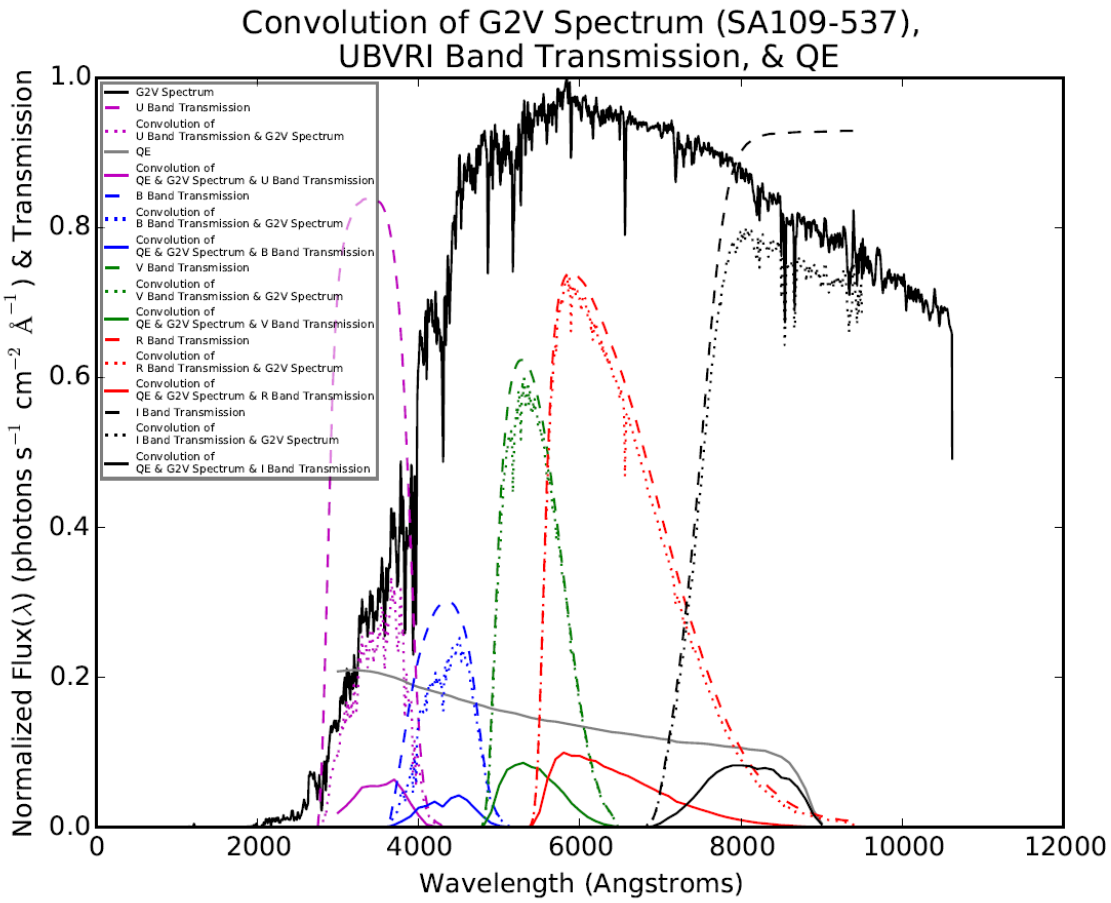

Fig. 4. Convolution of a G2V spectrum with the UBVRI transmission curves and the QE [9], after integrating results in synthetic instrumental fluxes for UBVRI that are arbitrarily scaled.

2.3 Transforming Landolt 2009 ([10]) Catalog UBVRI Magnitudes to Landolt's Measured Instrumental Fluxes

To anchor our synthetic instrumental fluxes in the UBVRI for a star to the Johnson-Cousins system we first need to calculate the measured instrumental fluxes in the UBVRI for that star from the catalog magnitudes of [10]. We use the following expression, Pogson's equation, from [19] relating magnitudes and fluxes,

$$m_1 - m_2 = -2.5*\log_{10}(F_1/F_2)$$

We will apply this general expression to calculate the measured instrumental flux as measured by Landolt's system, F_1.

$$m_1 - m_2 = -2.5*\log_{10}(F_1/F_2)$$

$$-(m_1-m_2)/2.5 = \log_{10}(F_1/F_2)$$

$$10^{-(m1-m2)/2.5} = \cancel{10}^{\cancel{\log 10}(F1/F2)}$$

$$F_1/F_2 = 10^{-(m1-m2)/2.5}$$

Yields the final expression,

$$F_1 = F_2 * 10^{-(m1-m2)/2.5}$$

which provides the measured instrumental flux as observed from Landolt's system of a standard star in [10]. m_1 is the in-band catalog magnitude for a standard star from [10], m_2 is the calibration star magnitude, F_1 is the standard star flux, and F_2 is the calibration star flux. The UBVRI system's magnitude zero points are set by defining Vega to have color indices of zero. The V magnitude of +0.03 mag implies that Vega then must be 0.03 mag in all bands [3] [17]. With subscript 2 as Vega, our calibration star, we use $m_2 = 0.03$ for all bands. F_2 is the only value left to be calculated to solve for F_1.

The spectrum of Vega (STIS_005) was retrieved from the Space Telescope Science Institute CALSPEC Calibration Database[5]. This Vega spectrum is flux calibrated and exo-atmospheric. The spectrum covers a wavelength range of 900 to 3000000 Angstroms, but only wavelengths from 2000 to 10000 Angstroms are used. The spectrum of Vega was converted from flux in energy units to flux in photon units in the same manner as done for the spectra from Pickles Spectral Library. The spectrum of Vega is shown in Fig. 5. The flux of Vega, F_2, is determined synthetically via modeling in the same fashion as the standard star spectra discussed previously. The flux calibrated spectrum of Vega is convolved with the U band transmission. The resulting convolution is then convolved with the [9] QE. The final convolution is integrated to provide the U band synthetic instrumental flux of Vega as observed by Landolt's system. This process is repeated for the B, V, R, and I bands. With the flux of Vega calculated, the measured instrumental flux of a standard star is found. The UBVRI measured instrumental flux of SA109-537 (a G2V spectral type) is shown below in Fig. 6. We use the pivot wavelengths from [15] to represent the x-axis wavelength of the UBVRI bands, the pivot wavelength is a source-independent wavelength of a filter [15].

[5] For more information see http://www.stsci.edu/hst/observatory/crds/calspec.html

Retrieved from ftp://ftp.stsci.edu/cdbs/calspec

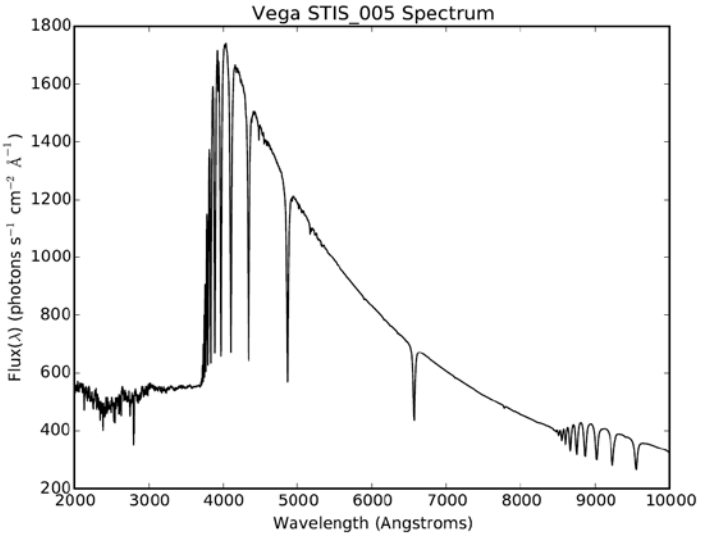

Fig. 5. Flux calibrated spectrum of Vega (STIS_005) used for calibration in the modeling.

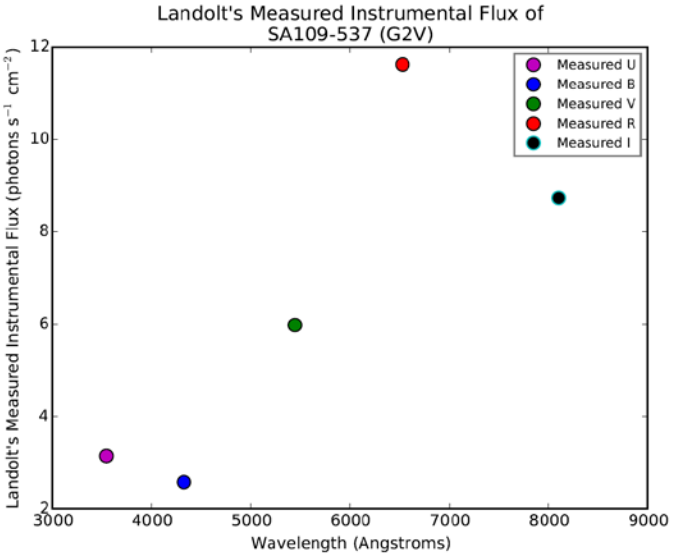

Fig. 6. Landolt's measured UBVRI instrumental flux for SA109-537, which has a spectral type of G2V.

[10] used nonlinear color term transformations as final step to put the new observations of [10] onto the photometric system defined in [9], these transformations can be found in [10] (their Table 1). These are color term corrections that are broken up into linear segments for different values of color index to approximate a polynomial relation. These nonlinear color term transformations were determined by comparing new observations of [10] to the data from [9]. Once these nonlinear color term transformations were applied they were then combined with the star data from [9] for the stars in common to create the final table of magnitudes and color indices, Table 2 of [10]. Due to [10] combining new observation data from [10] that has a nonlinear color term transformation to the [9] system with observation data from [9] which did not have this nonlinear color term transformation, we cannot remove the nonlinear color term transformation from the standard star data from Table 2 of [10]. This would theoretically be the

first step in taking a standard star catalog magnitude from [10] and converting it to Landolt's measured instrumental flux. However, the nonlinear color term transformations of [10] are typically less than 1%, less than 2% for B-V, and is largest at less than 4% for the U-B nonlinear color term transformation, based on nonlinear color term plots from [20], where [10] states that the nonlinear relations of [10] have the same overall general appearance as those of [20]. By not removing the nonlinear color term transformations in converting from catalog magnitudes to measured instrumental fluxes this may have an effect on our results of at most a few percent.

2.4 Putting Synthetic Instrumental Fluxes onto the Johnson-Cousins Photometric System

The measured instrumental flux of a standard star provides an anchor that will eventually place the synthetic instrumental flux of that standard star on the Johnson-Cousins photometric system. Since synthetic instrumental fluxes are arbitrary, they need to be calibrated. This calibration is performed by scaling them to the measured instrumental fluxes. To do this, we use a chi-squared-like test that yields a best fit between the synthetic instrumental fluxes and the measured instrumental fluxes for the BVRI bands. We chose the chi-squared-like expression from [21],

$$\chi^2 = \sum_{\lambda} \frac{[f_\lambda(measured) - f_\lambda(synthetic\ binary)]^2}{f_\lambda(measured)}$$

[21] uses this expression to compare a synthetic binary spectrum to a measured peculiar spectrum that is suspected of being an unresolved binary. We adapted this expression for our purposes to,

$$\chi^2 = \sum_{bands} \frac{[F(measured) - F(theory)]^2}{F(measured)}$$

F(measured) is the measured instrumental flux for some band n, F(theory) is the synthetic instrumental flux for band n, and the resultant expression is the individual chi-squared value for band n, where a summation over the bands yields the total chi-squared value. We create a grid of scaling values so that we can apply the chi-squared-like test to each one. For each value in this grid, the UBVRI synthetic instrumental fluxes were scaled to match the measured instrumental fluxes, chi-squared values for the UBVRI bands were calculated and then summed to give the total chi-squared value. The minimum total chi-squared value determined the best fit, and therefore determined the scaling. The U band was excluded from the total chi-squared value because this band has a larger discrepancy between the synthetic instrumental flux and the measured instrumental flux compared to the BVRI bands.

Fig. 7 shows the chi-squared values of SA109-537 (a G2V spectral type) as a function of scaling for the UBVRI bands, as well as the total chi-squared value that uses only the BVRI bands. The U band is only shown for completeness. Fig. 8 shows the measured instrumental fluxes (circles) of SA109-537 in the UBVRI bands and its synthetic instrumental fluxes (squares) in the UBVRI bands after applying the scaling factor. Scaling the UBVRI synthetic instrumental fluxes is equivalent to scaling the normalized spectrum of the standard star. Recall that a normalized spectrum has been scaled such that it has a peak value of one, i.e. it is not flux calibrated. The convolution process is a multiplicative process, so scaling by a constant will carry that constant through so it can be pulled outside of the integral. Scaling a normalized spectrum by a constant has the effect of scaling the UBVRI synthetic instrumental fluxes by the same constant. The scaling that results in a minimized chi-squared places the spectrum on the instrumental system of Landolt, simulating as if the standard star was observed by Landolt's system. Then the synthetic panchromatic instrumental flux is determined by convolving the scaled normalized spectrum of the standard star with the QE [9] and integrating. The synthetic panchromatic instrumental flux of Vega is determined by convolving the flux calibrated spectrum of Vega with the QE [9] and then integrating. No scaling factor is needed for the latter because the spectrum of Vega is flux calibrated. Using Pogson's equation, we calculate the final calibrated panchromatic magnitude of the star on the Johnson-Cousins photometric system. We repeat this

process for each star, deriving Open magnitudes on the Johnson-Cousins photometric system for all of the stars in our standard star catalog. Our catalog of derived Open magnitudes on the Johnson-Cousins photometric system can be found in Tab. 12 in the Appendix. This table has been made available for use by the community to calibrate panchromatic systems.

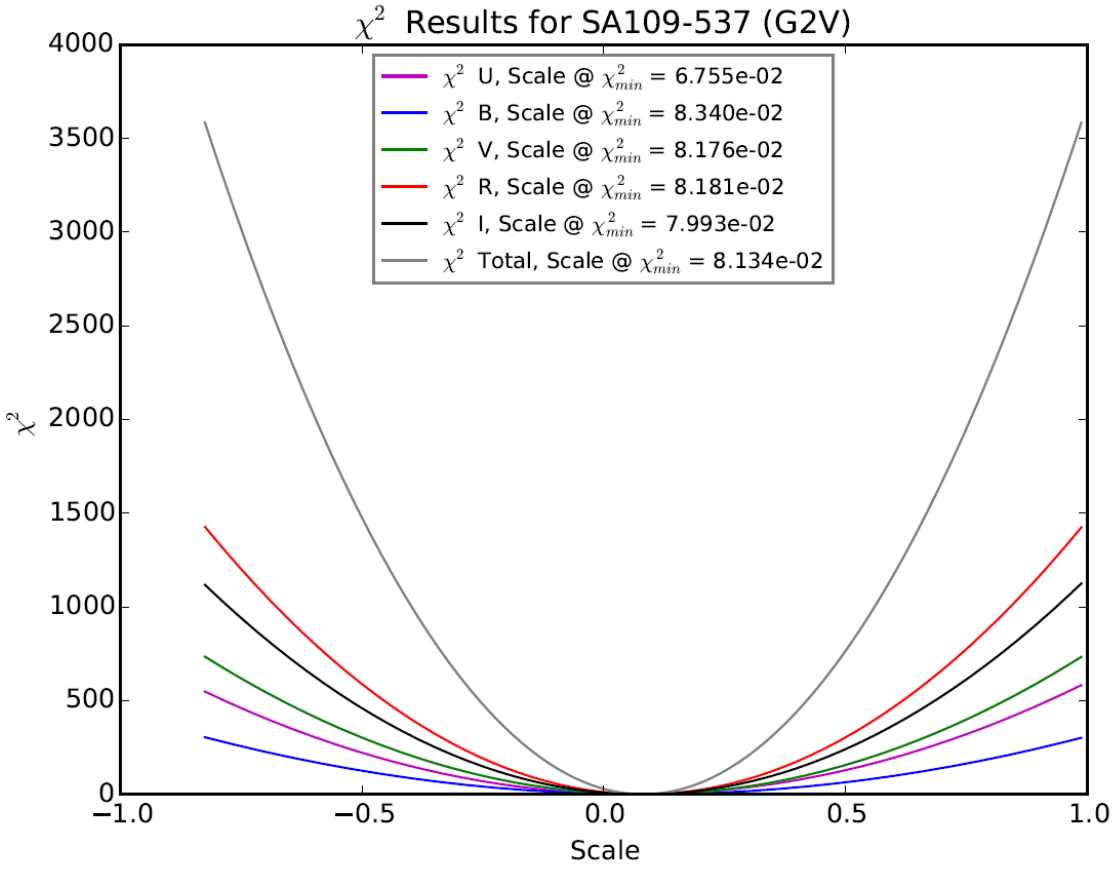

Fig. 7. χ^2 results for SA109-537, showing the scaling of the synthetic instrumental fluxes as a function of χ^2 to provide the best fit to the measured instrumental fluxes.

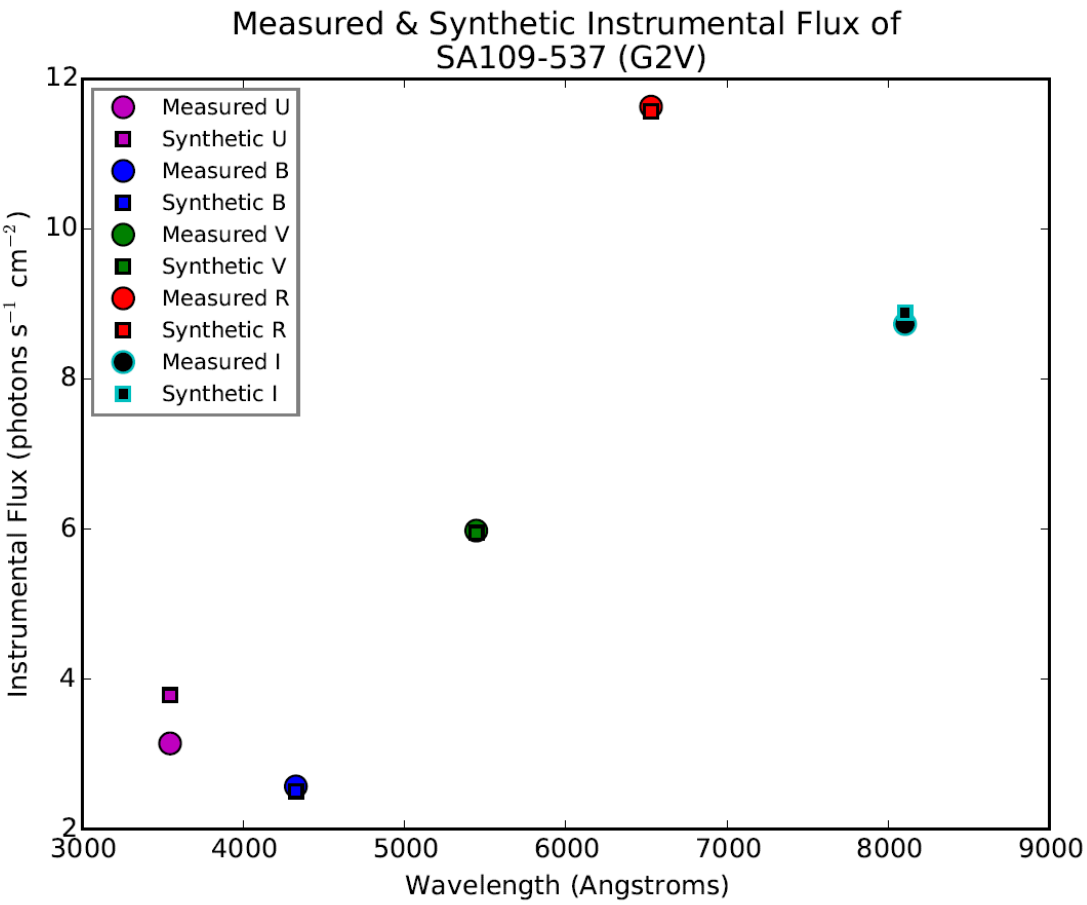

Fig. 8. UBVRI measured instrumental fluxes and the synthetic instrumental fluxes with the best fit scaling via the minimum total chi-squared result.

2.5 Calculating the Atmospheric Cutoff

The atmosphere becomes opaque at around ~ 3000 Angstroms [22] [17] [18]. The measured catalog magnitudes from [10], the spectra from Pickles Spectral Library, and the flux calibrated spectrum of Vega are all exo-atmospheric, they have been corrected for Earth's atmosphere. However, the U band extinction corrected photometry of [10] is the product of a U band transmission curve modified by the cutoff of the atmosphere. The Johnson U bandpass is partially determined by the atmosphere's ultraviolet cutoff [17]. Whereas the UBVRI filter transmission curves of [9] used for modeling do not include the atmospheric cutoff around ~ 3000 Angstroms. This is the most likely explanation for the U band synthetic instrumental flux being discrepant with the measured instrumental flux, as compared to the BVRI bands. To simulate an atmospheric cutoff we truncate the QE of [9]. To determine an effective atmospheric cutoff for the measured U band catalog data from [10], we perform the chi-squared like test on the U band. We perform this analysis using an atmospheric cutoff of 2900, 3000, and 3100 Angstroms, using a resolution of 100 Angstroms (the resolution of the QE of [9]). For each iteration of atmospheric cutoff we perform our chi-squared like test and total the U band chi-squared value for all of the stars. The smallest total U band chi-squared value for all of the stars for the grid of atmospheric cutoffs determines the optimal atmospheric cutoff that most closely represents that of the measured U band catalog data from [10]. The results of this analysis are shown in Fig. 9 below. The minimum total U band chi-squared value for all of the stars occurs at 3000 Angstroms. It is necessary to find the optimal atmospheric cutoff not to match the U band synthetic instrumental flux to the measured instrumental flux, since the scaling was done using only the BVRI bands, but to

provide an atmospheric cutoff that can be applied to the spectra of Pickles Spectral Library as well as the flux calibrated spectrum of Vega, since these spectra include flux shortward of ~3000 Angstroms. This process is what determined the atmospheric cutoff used to derive synthetic Open magnitudes.

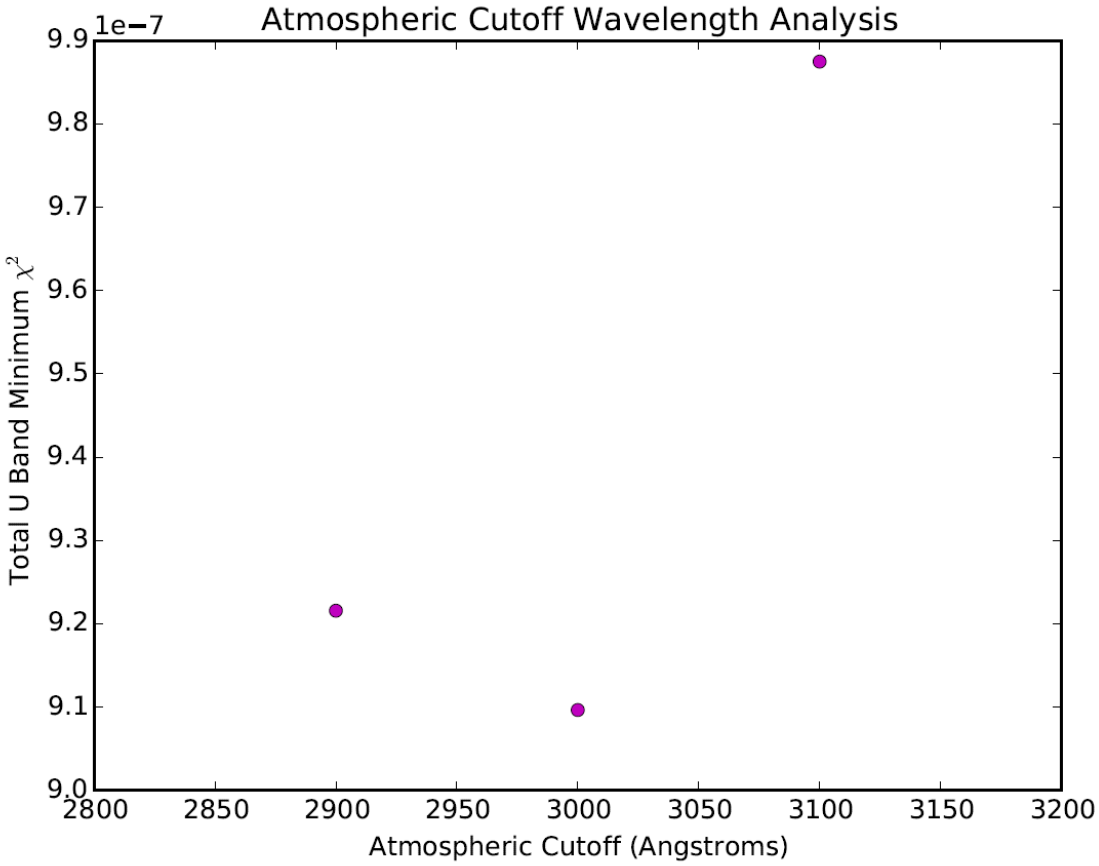

Fig. 9. Atmospheric cutoff wavelength analysis

2.6 Synthetic Open Magnitude

As one verification that our derived synthetic Open magnitudes are indeed on the Johnson-Cousins photometric system we compare the measured and synthetic magnitudes of an A0V star, SA98-653. Recall that for an A0V star the color indices are zero by definition, therefore the measured V magnitude of [10] should be the same as our Open magnitude. In reality, SA98-653 has measured color indices that are non-zero but small, with this star having the largest color index for U-B = -0.102, with the remaining indices as B-V = -0.003, V-R = +0.010, R-I = +0.009, and V-I = +0.017 [10]. A reasonable expectation for a difference between the measured V band magnitude and the synthetic Open magnitude based on the measured color indices would be perhaps < 0.03 mag (a few percent). Tab. 1 below shows the measured V band magnitude, our synthetic derived Open magnitude, and the difference between them. With the magnitude difference being small (1.0%), this provides evidence to support that our derived synthetic Open magnitudes are on the Johnson-Cousins photometric system.

Tab. 1. Comparison of Measured V band Magnitude and Synthetic Open Magnitude of SA98-653

Measured V Magnitude	Synthetic Open Magnitude	Magnitude Difference
9.538	9.528	0.010

Fig. 10 below shows a plot of the measured UBVRI photometry of [10] minus our derived synthetic Open magnitudes as a function of B-V. The difference between the V band and the Open is surprisingly small for a B-V of about 0 to 1.2, but begins to deviate outside of this range. The other bands deviate from the Open by a considerable amount. It is worthy to note that using a Johnson-Cousins V band catalog value as an estimate for the Open band catalog value is a reasonable approximation within the range where V – Open values are close to zero. While using standard stars outside of this B-V range for calibration purposes is ill-conceived for estimating the Open band magnitude.

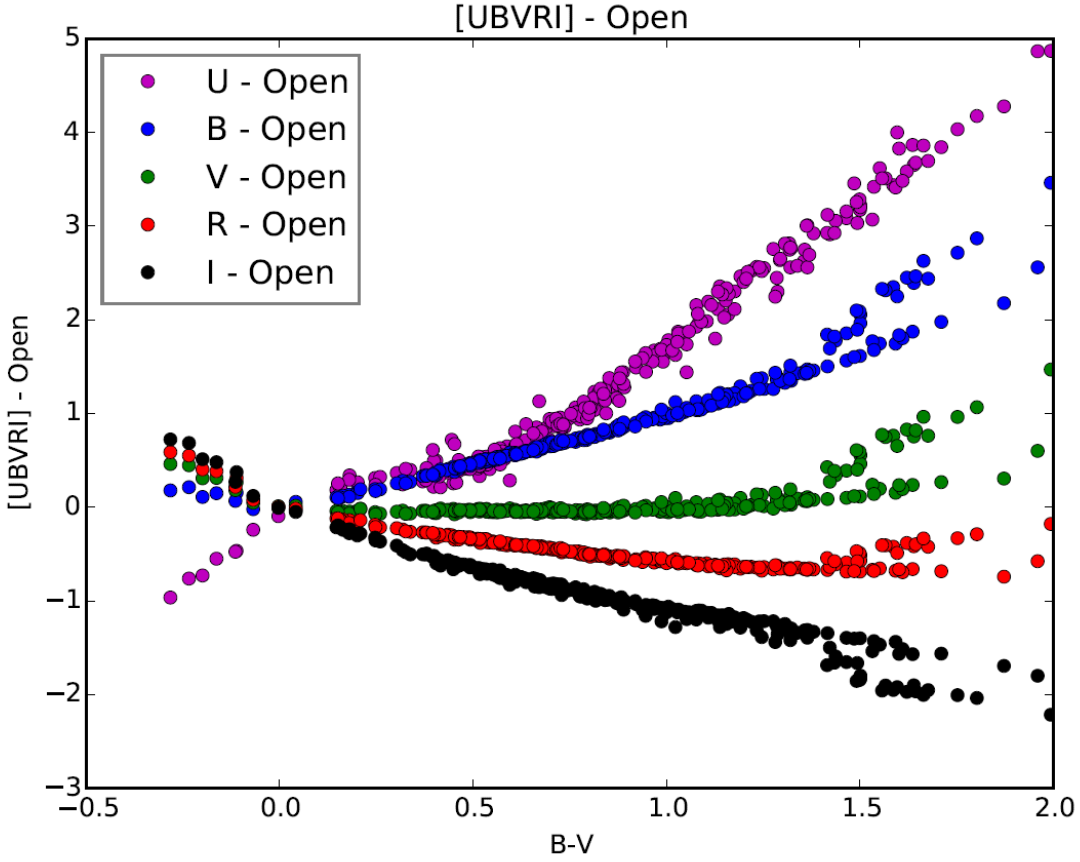

Fig. 10. Comparison of the synthetic Open magnitude derived in this work to the corresponding UBVRI in [10] for all the stars in our catalog.

The [BVRI] – Open splits at about B-V = 1.4, providing degenerate magnitude differences for a given B-V value. A further inspection as a function of luminosity class is shown in Fig. 11. Squares are luminosity class V, circles are class IV, triangles are class III, and stars are class II. There are no luminosity class I sources in our final standard

star catalog. With this plot it becomes clear that the split after about B-V = 1.4 is due to luminosity class, with the main sequence taking one branch and class II and III the other.

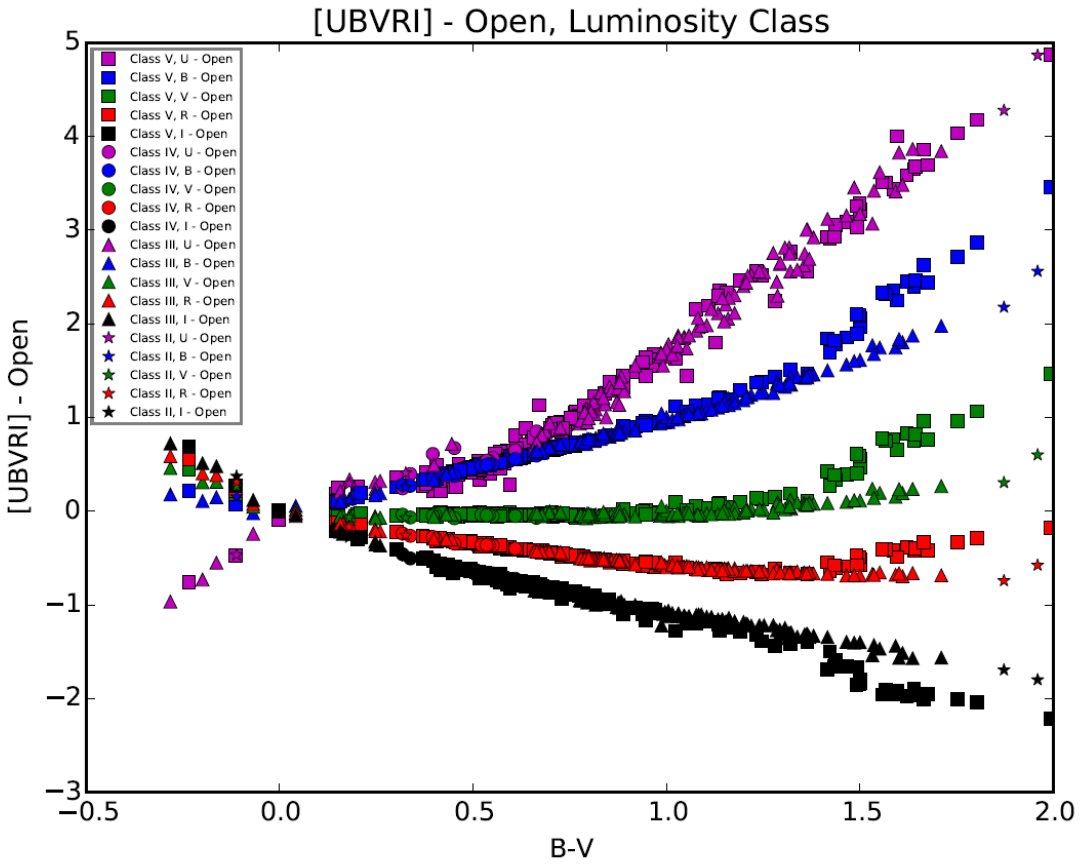

Fig. 11. Comparison of the synthetic Open magnitude derived in this work to the corresponding UBVRI in [10] for all the stars in our catalog, broken down into luminosity class.

3. OBSERVATIONS

3.1 John Bryan State Park Observatory

The John Bryan State Park Observatory (JBO) is located in John Bryan state park at latitude and longitude 39°47’37’’ N, 83°51’27’’ W, 305 meters above sea level. The John Bryan State Park Observatory houses two of the three observatories used for this paper, the Quad-axis Telescope and the Sliding Roof Observatory.

3.1.1 Quad-axis Telescope

The Quad-axis Telescope (Quad) is located at the John Bryan State Park Observatory. The telescope is a 24-inch Cassegrain telescope on a custom quad-axis mount designed by Dr. Ken Kissell in the 1960’s. The optics has an f/11 focal ratio with an open truss system and secondary baffling. The camera is an Apogee Alta U4000 with a 2048 x 2048 pixel detector, with a pixel size of 7.4 x 7.4 micron. The system has no filter wheel. The panchromatic

observations of this paper did not use a clear filter but were made without one (i.e. open). The field of view (FOV) is 8 x 8 arc-minutes, with a plate scale of 0.2 arc-seconds per pixel.

3.1.2 Sliding Roof Observatory

The Sliding Roof Observatory (SRO) is located at the John Bryan State Park Observatory. The telescope is a 16-inch MEADE LX200GPS Schmidt Cassegrain on an alt-az mount. The optics has an f/6.3 focal ratio and the camera is an Orion StarShoot G3 monochrome imager with a 752 x 582 pixel detector, with pixel size of 8.6 x 8.3 micron. The system has an Orion Nautilus 7 position filter wheel equipped with Astrodon filters. For the panchromatic observations of this paper we used the clear filter. The FOV is 12 x 9 arc-minutes, with a plate scale of 0.9 arc-seconds per pixel.

3.2 ROVOR

The Remote Observatory for Variable Object Research ([23]; ROVOR) is located in central Utah at 39°27'17.1'' N, 112°43'01.0'' W and 4579 feet above sea level. The telescope is an 0.4m RC Optical tube on a German-equatorial Paramount ME pier. The optics have an f/9 focal ratio in an open truss configuration with a primary mirror ion milled to 1/30 wave rms. The camera is an FLI ProLine PL003 with a back-illuminated 1024 × 1024 24 μm pixel SITe detector. The filter wheel is a 12 position FLI Centerline equipped with a set of 50 mm square Astrodon Johnson-Cousins BVRI and Sloan g'r'i'z' filters. The FOV is 23.4' on a side with a resolution of 1.37''/pixel. Pointing is accurate to better than 30'' within 45 degrees of the zenith.

3.3 Observation Plan

We performed panchromatic observations of satellites and standard stars to provide calibrated panchromatic satellite signatures. The purpose of this is to process and access the satellite signatures using theoretically derived open magnitudes on the Johnson-Cousins system.

The observation plan was performed by the three systems on the same night, July 11, 2016. Having the observations performed on the same night eliminates changes that may occur in the satellite signatures due to natural changes in the season or from satellite maneuvers. Having two systems at the same geographic location, Quad and SRO, eliminates any variables due to the atmospheric correction (all-sky calibrations provide an average extinction for the night), as well as differences in the observer's viewing angle of the target satellite that may result in differences in the satellite signature. A comparison of the satellite signatures from these two systems at the same geographic location will reveal any color terms due to the target satellite as evidenced by an offset between the signatures. Since the color index of the satellite is unknown at the time of observation we cannot apply a color term correction. This will provide an estimate of the size of the color term from the target satellite and therefore an estimate of the accuracy of the final photometry near the standard Johnson-Cousins photometric system when a color term for the target satellite is not included. The third geographically separate system will serve as a real world test in comparing calibrated panchromatic photometry from two different systems at different geographic locations. There may be additional differences in the signature compared to the signatures from the same geographic location due to different viewing conditions of the satellite. Since the night was photometric for both sites, any differences due to atmospheric correction are expected to be negligible. The geographically separate system, ROVOR, has a latitude that is extremely close to that of Quad and SRO, so the difference in viewing angles is only due to differences in longitude of the systems. By different viewing conditions of the satellite we mean that Quad and SRO will see a more easterly portion of the satellite and ROVOR will see a more westerly portion of the satellite. We expect variations in the signature due to viewing angle differences to be minimized compared to also having differences in

latitude of the geographically separated systems. The third geographically separate system will provide an estimate of the accuracy of calibrated panchromatic photometry of satellites under real world conditions.

3.3.1 Standard Stars

The standard stars used for calibrations are shown below in Tab. 2. These stars were chosen based a variety of criteria. A standard area (SA) was selected using the modified [10] catalog that was used to derive Open magnitudes on the Johnson-Cousins system. The criteria included the color index span of the stars, sufficient spatial separation of standard stars to observe them with all of the systems, being bright enough to obtain good signal-to-noise ratio (Vmag < 12), and spanning a sufficient range in airmass during the two-week observing window.

Tab. 2. Standard Star Observation Target List

Target	RA (J2000) [h:m:s]	Decl. (J2000) [d:m:s]	V [mag]	B-V [mag]	B-R [mag]
SA109-71	17:44:06.792	-00:24:58.01	11.49	+0.326	0.513
SA109-381	17:44:12.269	-00:20:32.80	11.731	+0.704	1.131
SA109-231	17:45:19.964	-00:25:51.60	9.333	+1.465	2.252
SA109-537	17:45:42.448	-00:21:35.43	10.353	+0.609	0.985

The calibrations for the night were determined by performing all-sky calibrations. All-sky calibrations are performed by observing standard stars at varying airmasses throughout the night. We performed this the same night as our satellite observations by observing the standard stars intermittently with the target satellites. This ensured that the calibrations obtained (zero point and extinction coefficient) were representative of the night of the satellite observations.

3.3.2 Satellite Targets

The satellite targets for the observation plan are shown below in Tab. 3. These targets were chosen by looking for lone satellites in the sky and with the system observing constraints. The lone satellites rather than using a satellite in a cluster will minimize the risk of there being a satellite cross tag. The system constraints were to have the target above the elevation limits of all of the observatories, and to have the targets on one side of the meridian to avoid meridian flips during the observing run. These were the three geosynchronous earth orbit (GEO) satellites that met the criteria. The color indices of the satellites were estimated using GCPC version 3m using all available data for each satellite. Galaxy-19 is solar color, Galaxy-25 is blue, and Galaxy-28 is red, based on the B-R color index. Galaxy-25 is red, Galaxy-28 is solar color, based on the B-V color index, while Galaxy-19 did not have V band data available to calculate a B-V color index. The standard deviation, σ, is given for the B-V color index. Both Galaxy-19 and Galaxy-25 have the same bus type, while Galaxy-28 has a similar bus type. The satellites span an age range of about a decade, with Galaxy-25 being the oldest. These targets are similar in bus type but span a considerable range in age and color index. The color index of a satellite is important in that the offsets of the satellite signatures between the three different systems may be a function of color term and therefore a function of color index.

Tab. 3. Satellite Target List

Target	NORAD ID	Average B-V [mag]	σ(B-V) [mag]	Median B-V [mag]	Average B-R [mag]	Median B-R [mag]	Bus Type[6]	Launch Date[6] [year-month-day]
Galaxy-19	33376	N/A	N/A	N/A	1.13	1.17	SSL-1300	2008-09-24
Galaxy-25	24812	0.97	0.15	0.98	0.97	1.03	SSL-1300	1997-05-24
Galaxy-28	28702	0.66	0.12	0.67	1.38	1.39	SSL-1300S	2005-06-23

3.3.3 Vega-like Star SA114-750

In order to provide an empirical determination of the Open magnitude to compare with the theoretically derived Open magnitudes, it is necessary to put the observations on the Johnsons-Cousins photometric system. This requires a Vega-like star, or a star of spectral type of A0V. The Johnson-Cousins system defines Vega as having color indices of zero such that the magnitude in each band is the same by definition. This also means that the magnitude in the Open is also the same as the in-band (UBVRI) magnitudes. A search of [10] was performed for Vega-like stars using the constraint of having the B-V, V-R, R-I, and V-I color indices within 0.1 of zero while ignoring the U band. The best star meeting these requirements available to observe (within a specific range of observable right ascension (RA)) was SA114-750. This star from [10] meets our requirements for a standard star discussed earlier; photometric error, and number of nights and number of times the star was observed. The details of SA114-750 are shown in Tab. 4 below, from [10] unless otherwise noted. The largest deviation from zero for a color index is B-V = -0.037 if we don't include the U band. If we include the U band the U-B is the largest deviation at -0.367. While this was not the most ideal target, it was the best option available at the time of our observation window. We use SA114-750 as a calibration star to put our standard star observations onto the Vega system so that we have an empirical measurement in the Open that is almost on the Johnson-Cousins system. Note that it will not truly be on the Johnson-Cousins system since the observations were done using a system other than Landolt's. To fully place the observed magnitudes on the Johnson-Cousins system, a color term between the system that made the observations and Landolt's system will have to be applied. The four standard stars we have observed will provide a test of the validity of the theoretically derived synthetic Open magnitudes by comparing them to the empirically determined Open magnitudes.

Tab. 4. Details of SA114-750

Star Name	RA (J2000) [h:m:s]	Decl. (J2000) [d:m:s]	Spectral Type	V [mag]	B-V [mag]	U-B [mag]	V-R [mag]	R-I [mag]	V-I [mag]
SA114-750	22:41:44.703	+01:12:36.36	B9[7], A0IV[8]	11.916	−0.037	−0.367	+0.027	−0.016	+0.010

3.3.4 Observation Schedule

One of the goals of the observation schedule was to obtain overlapping observations of the satellites and standard stars such that the result would be satellite signatures that overlap in longitudinal phase angle (LPA) for each system. For this to occur, an observation plan was created to allow each system to follow a scheduled sequence of standard star observations and satellite observations.

[6] From Gunter's Space Page, http://space.skyrocket.de/
[7] From [49]
[8] From [47], with a poor 'fit rank' of 6

Calibration frames were obtained for each system before or after the targets were observed. This includes bias frames, dark frames, and flat frames. A sufficient number of each calibration frame was taken to create a statistically relevant master frame. Dark frames were taken of the same exposure as the frames being dark subtracted for the Quad and SRO, while the master dark of ROVOR was applied via a linear scaling after verifying that the dark current for the ROVOR is indeed linear.

Standard star observations were performed every hour starting at astronomical twilight until SA109 was below 30 deg elevation (> 2 airmass). The beginning of the observing schedule for ROVOR was slightly offset from astronomical twilight to align slightly better with the Quad and SRO. In between standard star observations the satellite targets were observed. During satellite observations, several exposures were taken of the first target satellite, several exposures of the second target satellite, and then several exposures of the third target satellite. This process was repeated until the next standard star observation was scheduled. This sequence of standard star and satellite observations ended around astronomical dawn. SA114-750 was observed near astronomical dawn, about ten exposures were taken using each system. Satellite observations continued afterward for about a half hour after astronomical dawn while the sky brightness still allowed for a good signal-to-noise ratio of the targets. The exposure time on targets was such as to obtain nominal signal-to-noise ratio, aiming for < 0.01 mag error.

3.4 Data Reduction

Our image reduction for each system consisted of 1) create the master bias frame; 2) Subtract the master bias frame from the data, dark, and flat-field frames to obtain data', dark', and flat-field'; 3) Create the master dark frame.; 4) Scale the master dark to the exposure time of data and flat-field and subtract from them to get data'' and flat-field''; 5) Create the master flat-field frame; 6) Divide data'' by master flat-field. Or,

1. Create master bias frame
2. $data' = data - masterbias$
2. $dark' = dark - masterbias$
2. $flatfield' = flatfield - masterbias$
3. Create master dark frame
4. $data'' = data' - \alpha\ masterdark$
4. $flatfield'' = flatfield' - \beta\, masterdark$
5. Create master flat-field frame
6. $$data''' = \frac{data''}{masterflatfield}$$

The α and β are scaling factors to adjust the dark frame to an equivalent dark that one would obtain with the same exposure as the frame being reduced [24] [22].

3.5 Photometry Primer

We use the following expression to obtain calibrated photometry,

$$m_{standard} = m_{inst} + m_{ext} + m_{zp} + m_{color\_term}$$

- $m_{standard}$ is the magnitude on a standardized system, for this paper that is the Johnson-Cousins photometric system. This magnitude is referred to as a calibrated magnitude.

- m_{inst} is the instrumental magnitude,
    - $m_{inst} = -2.5*\log_{10}(flux_{target})$. = $-2.5*\log_{10}$(net electrons/exposure time). Net electrons is the net counts from the target multiplied by the gain of the camera, and exposure time is the length of integration of the target on the detector.
- m_{ext} is the amount of light not reaching the telescope due to the atmosphere. After applying this we say the resulting magnitude is exo-atmospheric.
    - $m_{ext} = -k*X$, k is the extinction coefficient in units of mag airmass^{-1}, X is the airmass
    - This term may be calculated by finding the slope from a plot of airmass versus $m_{catalog} - m_{inst}$ for standard star observation data. This technique uses observations of standard stars throughout the night spanning a range of airmass. The expression $m_{standard} = m_{inst} + m_{ext} + m_{zp} + m_{color\_term}$ turns into, $m_{standard} - m_{inst} = -k*X + m_{zp} + m_{color\_term}$, which has the form y = mx + b. The left hand side is the y-value, the -k value is the slope, the X is the x-value, and the $m_{zp} + m_{color\_term}$ is the y-intercept. By solving for the slope of the data we can find the extinction coefficient (k).
- m_{zp} is the zero point magnitude, and is a part of the transformation from the instrumental system to the standard system
    - see m_{color_term} for how this term is calculated
- m_{color_term} is the color term, a part of the transformation from the instrumental system to the standard system that is a function of color. This is to compensate for spectral response differences between the observers system and that of the Johnson-Cousins photometric system. For UBVRI photometry this value is often small (i.e. a few percent), while for panchromatic photometry we are sampling a much larger wavelength range where the differences in spectral response may have a more profound effect.
    - $m_{color\_term} = T*(CI)$, where T is the color coefficient and CI is the color index, (for example, B-V)
    - This term may be calculated in a similar fashion as the extinction coefficient (k), and uses the same observations of standard stars used to calculate the extinction coefficient (k). The expression $m_{standard} = m_{inst} + m_{ext} + m_{zp} + m_{color\_term}$ turns into, $m_{standard} - m_{inst} - m_{ext} = m_{zp} + m_{color\_term}$, which then turns into, $m_{standard} - m_{inst} + k*X = m_{zp} + T*(CI)$, which has the form y = mx + b. The left hand side is the y-value, T is the slope, CI is the x-value, and m_{zp} is the y-intercept.

Finally we have,

$$m_{standard} = -2.5*\log_{10}(flux_{target}) - k*X + T*(CI)$$

We note that we ignore the second order extinction correction in our calibration expression. The justification for this is discussed in more detail in Section 4.2.

Another way to express instrumental magnitude, from the perspective of image extraction is,

$$m_{inst} = -2.5*\log_{10}(flux_{target}) = -2.5*\log_{10}(\text{net electrons/exposure time})$$

One way to calculate net counts is by using a circular extraction region called an '**aperture**'. The aperture adds up all the light from the target, the '**signal**' (target counts + background counts). The aperture is large enough to capture virtually all of the light from the target (~ 3 FWHM). An annulus centered on the aperture and larger than the aperture is used to estimate the local **background** (units of counts per pixel^2). Where the net counts is found as,

net counts [counts]= **signal** [counts] – (**background** [counts pixel^{-2}] * **aperture** area [pixel^2]),

where the units are shown in brackets. And finally net counts is converted to electrons via gain of the camera,

net electrons = net counts * gain,

where gain has units of electrons counts^{-1}. The above process was applied to all of the observations discussed in this paper using the same custom software package called MIPS (Multispectral Image Processing Software). MIPS

performed aperture photometry on the standard stars to obtain calibration terms, extinction coefficients (k), zero point magnitudes (m_{zp}), color terms (T*(CI)), as well as on the satellites, to provide final results of calibrated panchromatic photometry of satellites.

4. RESULTS

4.1 Color Term of Standard Stars

The color term was calculated for each system, Quad, SRO, and ROVOR, to take into account the spectral response differences between each system and that of the Johnson-Cousins photometric system. The color term plots are shown below in Fig. 12, Fig. 13, and Fig. 14.

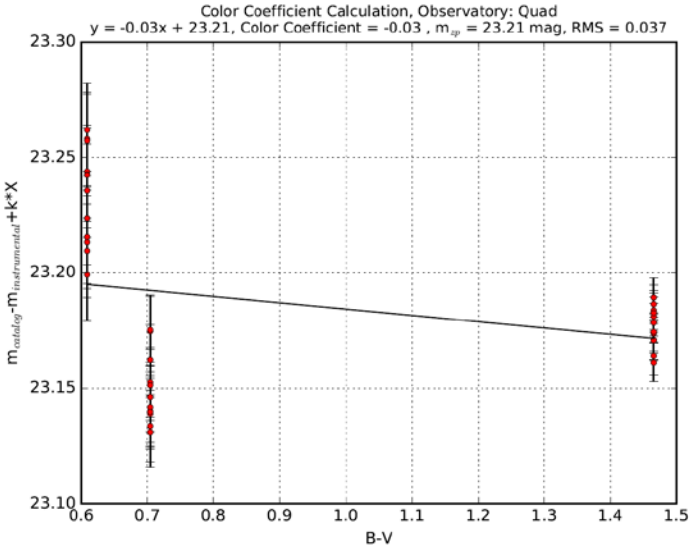

Fig. 12. Color coefficient plot for Quad.

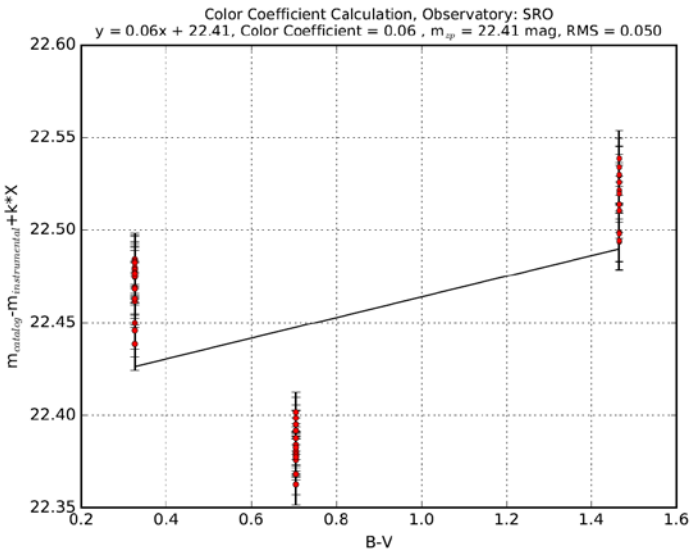

Fig. 13. Color coefficient plot for SRO.

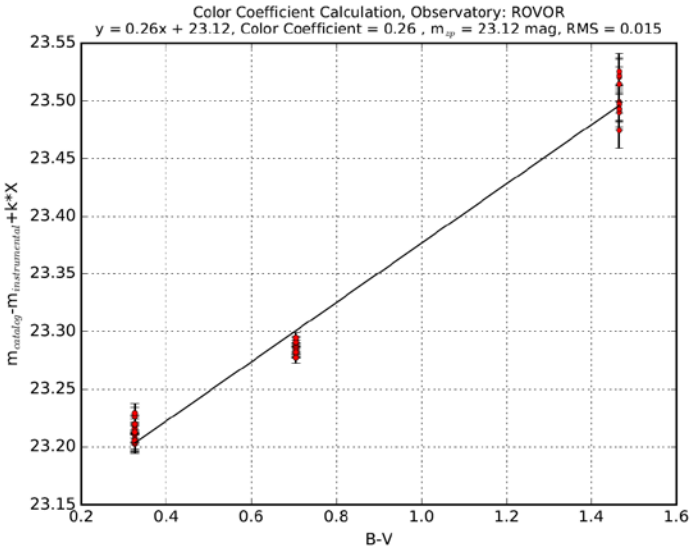

Fig. 14. Color coefficient plot for ROVOR.

4.2 Final Calibrations

The final calibration results for each system from the all-sky calibrations of the standard stars is shown below in Tab. 5, Tab. 6, and Tab. 7. The star with the largest RMS error was excluded from the calibrations, this is indicated in each table by the row with the strikethrough. Note that the color coefficient for Quad is close to zero, for SRO slightly larger, and for ROVOR significantly larger.

Tab. 5. Calibration Results for Quad

Quad			Color Coefficient = -0.03	Color RMS = 0.037			m_{zp} = 23.21
	Star	Extinction Coefficient (k)	m_{zp} + T*(B-V)	RMS Error	B-V	Color Term	m_{zp}
	~~SA109-71~~	~~0.12~~	~~23.14~~	~~0.037~~	~~0.326~~	~~-0.01~~	~~23.15~~
	SA109-381	0.14	23.15	0.014	0.704	-0.02	23.17
	SA109-231	0.15	23.18	0.008	1.465	-0.04	23.22
	SA109-537	0.20	23.23	0.020	0.609	-0.02	23.25
	average	0.16	23.19				23.21
				Final Error = 0.045			

Tab. 6. Calibration Results for SRO

SRO			Color Coefficient = 0.06	Color RMS = 0.050			m_{zp} = 22.41
	Star	Extinction Coefficient (k)	m_{zp} + T*(B-V)	RMS Error	B-V	Color Term	m_{zp}
	SA109-71	0.19	22.47	0.014	0.326	0.02	22.45
	SA109-381	0.14	22.38	0.010	0.704	0.04	22.34
	SA109-231	0.14	22.52	0.015	1.465	0.09	22.43
	~~SA109-537~~	~~0.17~~	~~22.50~~	~~0.031~~	~~0.609~~	~~0.04~~	~~22.46~~
	average	0.16	22.46				22.41
				Final Error = 0.055			

Tab. 7. Calibration Results for ROVOR

ROVOR			Color Coefficient = 0.26	Color RMS = 0.015			m_{zp} = 23.12
	Star	Extinction Coefficient (k)	m_{zp} + T*(B-V)	RMS Error	B-V	Color Term	m_{zp}
	SA109-71	0.14	23.21	0.008	0.326	0.08	23.13
	SA109-381	0.13	23.29	0.004	0.704	0.18	23.11
	SA109-231	0.13	23.50	0.015	1.465	0.38	23.12
	~~SA109-537~~	~~0.09~~	~~23.22~~	~~0.016~~	~~0.609~~	~~0.16~~	~~23.06~~
	average	0.13	23.33				23.12
				Final Error = 0.023			

The second order extinction correction was found to be negligible and therefore set to zero. The second order extinction is the result of blue objects fading faster than red objects as they approach the horizon. The second order extinction term accounts for excess fading of an object that is bluer. The second order extinction correction can be expressed as, k''*CI*X, where, k'' is the second order extinction coefficient, CI is the color index, and X is the airmass [8] [17]. [25] shows that the second order extinction coefficient for the B band is small, and on the order of -0.04 airmass^{-1} or less, and is largely constant; while the V, R, and I band second order extinction correction is quite small and can usually be ignored [17]. We find no evidence of second order extinction present in our panchromatic data. The two stars, SA109-381 and SA109-231, with different B-V color indices, Δ(B-V)~ 0.8 mag, had the same or very similar extinction coefficients, as seen in Tab. 5, Tab. 6, and Tab. 7 for each system. Although these two stars are not necessarily blue and red compared to the solar color index, one is solar and one is red in the B-V color index. Note that [25] uses a solar color index star and a red color index star as a blue-red pair to calculate the second order extinction coefficient. Based on this we set the second order extinction correction to be zero throughout this paper for our analysis. For more details regarding the second order extinction correction see [8], [17], and [25].

Fig. 15 below shows the normalized QE curves of all the CCDs, the QE defining the Johnson-Cousins photometric system of [9] (gray solid line), Quad (Apogee Alta U4000, blue dashed line), SRO (Orion StarShoot, red dash dot line), and ROVOR (SITe, green dotted line). The Quad QE collects less flux from a target than the [9] QE shortward of 4000 Angstroms, more flux from 4000 to ~6250 Angstroms, less flux from ~6250 to 9000 Angstroms, and more flux longward of 9000 Angstroms. It is not difficult to imagine the net effect of this producing a color coefficient close to zero. Comparing the SRO QE to the Quad QE, the curves are not too dissimilar with SRO being slightly redder. SRO collects less flux than Quad below 4500 Angstroms, and more flux from 5000 to 10,000 Angstroms. SRO overall collects more flux in the red than does Quad, and therefore SRO has a slightly larger color coefficient than Quad. Comparing the ROVOR QE to the Quad QE, the curves are quite dissimilar with ROVOR in general being significantly redder. ROVOR collects less flux from ~4000 to ~5500 Angstroms, and significantly more flux from ~5500 to 11000 Angstroms. ROVOR overall collects significantly more flux in the red than does Quad, and therefore it is consistent that ROVOR has a significantly larger color coefficient than Quad.

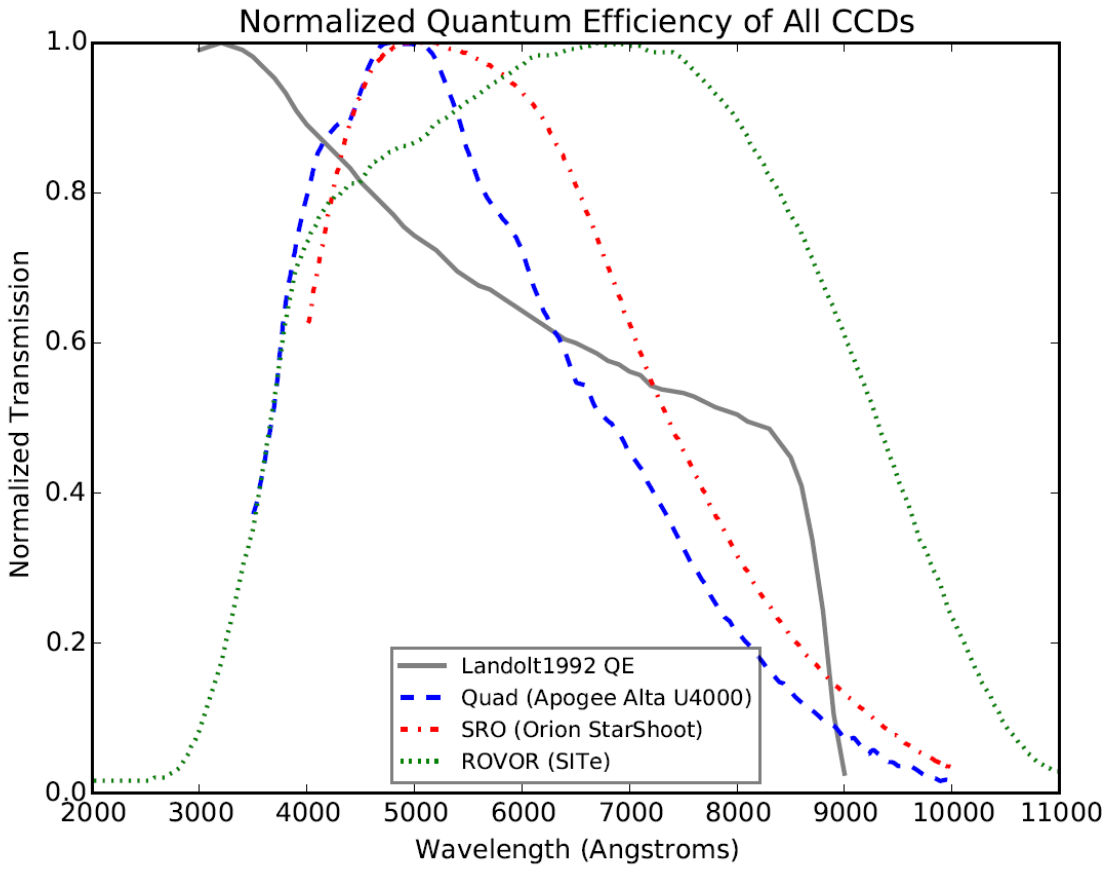

Fig. 15. Normalized QEs of all CCDs.

We note that using a common arbitrary Open magnitude (a dummy magnitude) for a standard star for the purposes of calibration between observations from different systems will indeed provide calibrated photometry that is close to 'some' system, with a color term putting it completely on 'some' system. But the calibrated photometry will not be on a 'standard system'. These calibrated results will not have physical meaning since they are not calibrated to a known object, such as the Johnson-Cousins photometric system which is calibrated to Vega.

4.3 Satellite Signatures

We have already taken the color term for the stars into account to properly calculate the zero point magnitude, m_{zp}. With the calibrations determined using the standard stars, extinction coefficient (k) and zero point magnitude (m_{zp}), we can now calculate the magnitude of the satellites on the standard system. However, the color term associated with each satellite is unknown since the color index of each satellite throughout the night of our observations is unknown, we are observing with a panchromatic system. Therefore, the expression used in the standard star calibrations is modified and the color term is removed since it is not known.

The satellite signatures between Quad and SRO, two systems at the same site, should overlap except for any color term that was not taken into account. The offset between Quad and SRO for a satellite is representative of the color term for that satellite between the two systems. The offset between Quad/SRO and ROVOR, where ROVOR is

geographically separate from Quad/SRO, is representative of a color term and geographic differences. The geographic differences can be broken up into atmospheric, and location, where location can further be broken up into distance between site and satellite, and viewing angle of the satellite. Since both sites had very photometric nights we assume that the calibrations of the atmosphere, the average extinction coefficient, is representative of the night and was properly taken into account. We can remove the effect of distance between the observing site and satellite by range normalizing the exo-atmospheric magnitude of the satellite. This leaves only color term and viewing angle as factors that could result in an offset between Quad and ROVOR or SRO and ROVOR. We note that the angular separation between ROVOR and JBO (Quad and SRO) as viewed from each satellite's perspective is ~ 3.5 deg.

In Fig. 16, Fig. 18, and Fig. 20 below we show the range normalized satellite signatures for Galaxy-19, Galaxy-25, and Galaxy-28, respectively. Fig. 17, Fig. 19, and Fig. 21 below show the same plots but with error bars, respectively. For each satellite, the three system satellite signatures are shown, Quad (blue circle), SRO (red square), and ROVOR (green triangle). We range normalize the exo-atmospheric calibrated magnitude using 36,000 km, the approximate altitude of a GEO satellite, a typical value for range normalizing GEO satellites. We note that the effect of range normalizing the exo-atmospheric magnitudes relative to these two sites is quite small, with the largest relative change between the two sites for a satellite being about 0.02 mag.

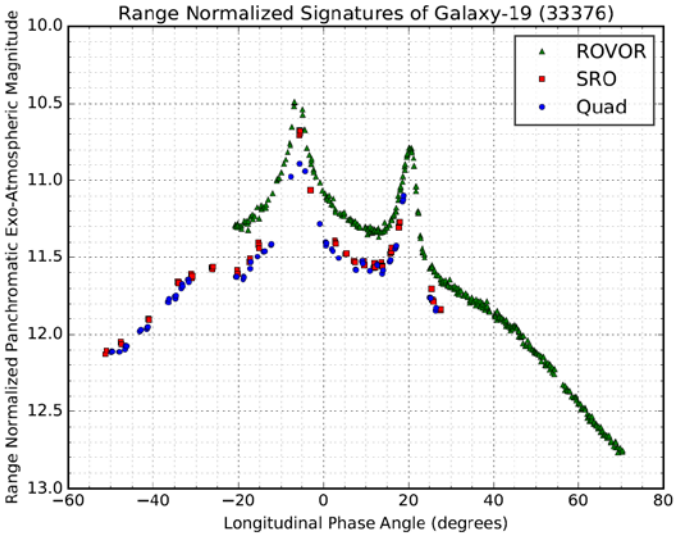

Fig. 16. Range normalized signatures of Galaxy-19 (33376).

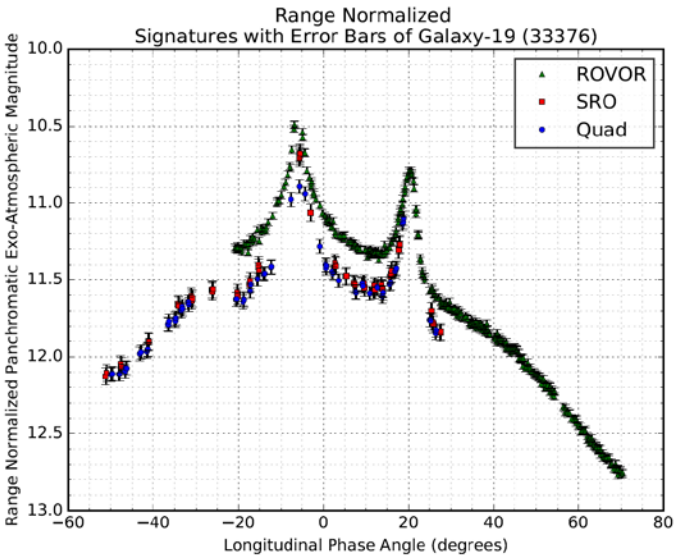

Fig. 17. Range normalized signatures with error bars of Galaxy-19 (33376).

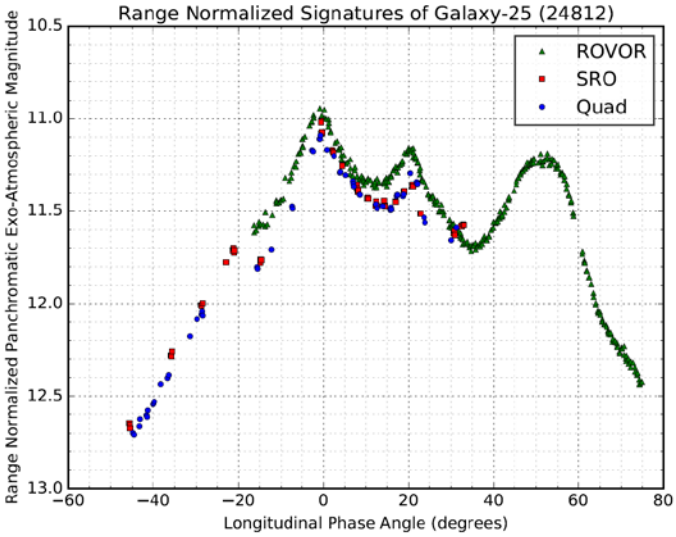

Fig. 18. Range normalized signatures of Galaxy-25 (24812).

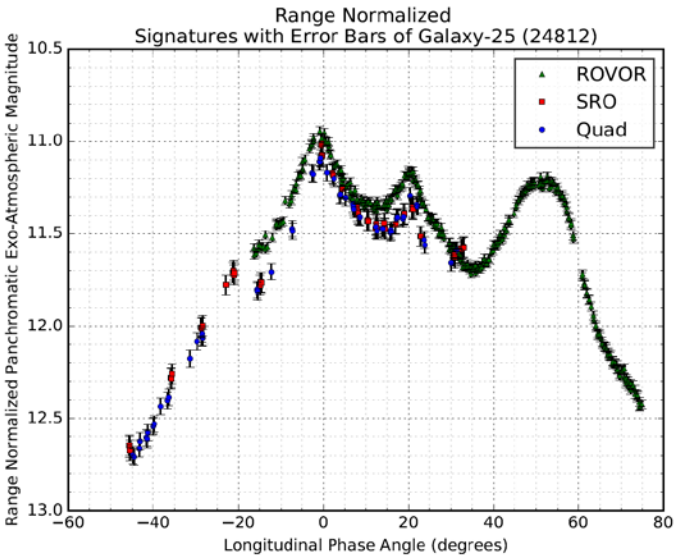

Fig. 19. Range normalized signatures with error bars of Galaxy-25 (24812).

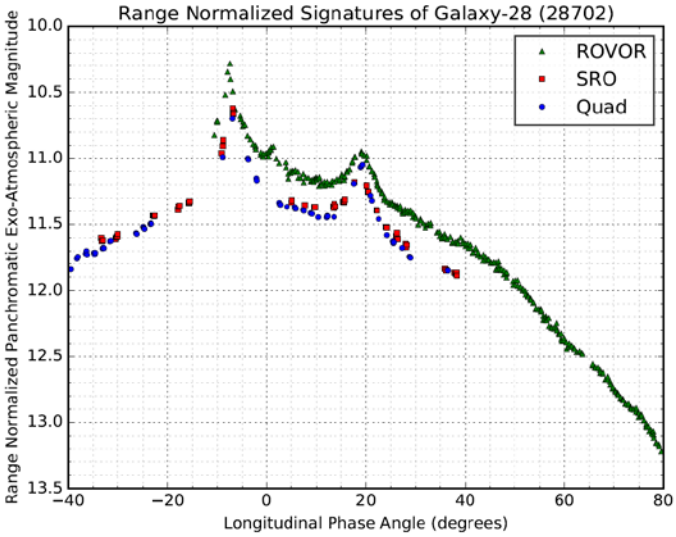

Fig. 20. Range normalized signatures of Galaxy-28 (28702).

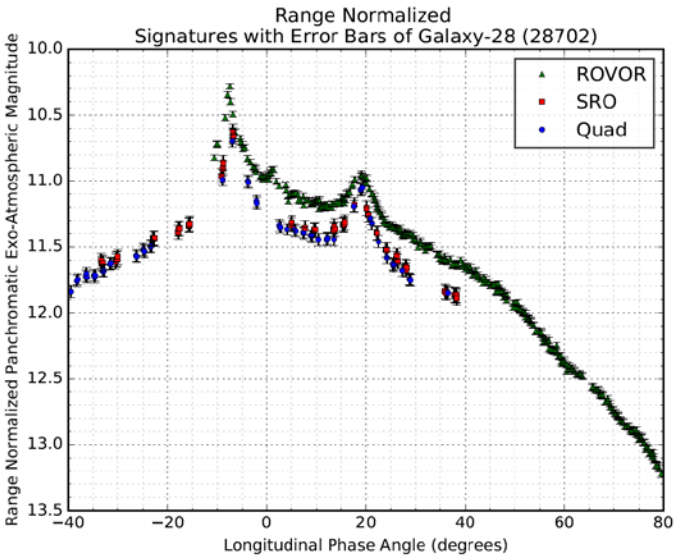

Fig. 21. Range normalized signatures with error bars of Galaxy-28 (28702).

The Galaxy-19, Galaxy-25, and Galaxy-28 plots show the signatures for Quad and SRO to be comparable, within the error bars. Since the only factor contributing to an offset between Quad and SRO can be the color term, and the color coefficients for Quad and SRO are similar, it is then reasonable for the offset or color term between them to be small.

The Galaxy-19, Galaxy-25, and Galaxy-28 plots show that the signatures for Quad and ROVOR, and the signatures for SRO and ROVOR, show a distinct offset, well outside of the error bars for the vast majority of the data. The

offset between Quad and ROVOR, and the offset between SRO and ROVOR may be the result of two factors, color term and viewing angle differences.

If the offset between two signatures were attributable to color term only we could derive the following. Using the equation from earlier,

$$m = m_{inst} + m_{ext} + m_{zp} + m_{color\_term}$$

If we apply this to system 1 and system 2 we get,

$$m_1 = m_{inst\_1} + m_{ext\_1} + m_{zp\_1} + m_{color\_term\_1}$$

$$m_2 = m_{inst\_2} + m_{ext\_2} + m_{zp\_2} + m_{color\_term\_2}$$

If the two systems were at different geographic locations such that the distance between the site and the satellite differed, the difference in site-satellite distance could be removed by calculating the range normalized magnitude from the exo-atmospheric magnitude via the expression (modified from [19]),

$$m - M = 5*\log_{10}(r/d)$$

$$M = m - 5*\log_{10}(r/d)$$

where m is the exo-atmospheric magnitude, M is the range normalized exo-atmospheric magnitude, r is the distance to the target in km, and d is the normalization distance of 36,000 km. The conversion to range normalized is an additive effect. It modifies our equations as shown below.

$$M_1 = m_{inst\_1} + m_{ext\_1} + m_{zp\_1} + m_{color\_term\_1} - 5*\log_{10}(r_1/d)$$

$$M_2 = m_{inst\_2} + m_{ext\_2} + m_{zp\_2} + m_{color\_term\_2} - 5*\log_{10}(r_2/d)$$

The color terms are for the satellites, but these are unknown so we set $m_{color\_term\_1}$ and $m_{color\_term\_2}$ equal to zero, to calculate a numerical answer for magnitude. This is what is plotted as the satellite signatures. If we take the difference between these, or the offset between data points of two different systems' satellite signatures, we have,

$$M_1' - M_2' = (m_{inst\_1} + m_{ext\_1} + m_{zp\_1} - 5*\log_{10}(r_1/d)) - (m_{inst\_2} + m_{ext\_2} + m_{zp\_2} - 5*\log_{10}(r_2/d)) = \text{offset}$$

Note that because we did not apply a color term and assumed it to be zero (incorrectly), the signatures are not yet on the Johnson-Cousins system, so we denote the magnitudes with a prime. If we did apply the color terms we would have calibrated magnitudes that were on the Johnson-Cousins photometric system and therefore the offset between data points of the signatures would be negligible and they would overlap (assuming that the viewing angle differences are negligible), or,

$$0 = M_1 - M_2 = (m_{inst\_1} + m_{ext\_1} + m_{zp\_1} + m_{color\_term\_1} - 5*\log_{10}(r_1/d)) - (m_{inst\_2} + m_{ext\_2} + m_{zp\_2} + m_{color\_term\_2} - 5*\log_{10}(r_2/d))$$

$$0 = (m_{inst\_1} + m_{ext\_1} + m_{zp\_1} - 5*\log_{10}(r_1/d)) - (m_{inst\_2} + m_{ext\_2} + m_{zp\_2} - 5*\log_{10}(r_2/d)) + (m_{color\_term\_1} - m_{color\_term\_2})$$

$$0 = M_1' - M_2' + (m_{color\_term\_1} - m_{color\_term\_2})$$

$$0 = \text{offset} + (m_{color\_term\_1} - m_{color\_term\_2})$$

$$\text{offset} = (m_{color\_term\_2} - m_{color\_term\_1})$$

Using the expression for color term,

$$m_{color\_term} = T*CI$$

We then have,

$$\text{offset} = (T_2*CI - T_1*CI)$$

$$\text{offset} = (T_2-T_1)*CI$$

If we take the average offset, noting that (T_2-T_1) is a constant, we finally have,

$$\text{average(offset)} = (T_2-T_1)*\text{average(CI)}$$

The offset between Quad and ROVOR, and the offset between SRO and ROVOR is attributed to two factors, color term and viewing angle differences, both of which are unknown. If for the moment we assume the contribution from viewing angle differences is negligible and the offset is due purely to the color term we can calculate the color index for the satellites and compare them to the GCPC historical database. Comparable color indices would indicate that the color term contribution to the offset was dominant compared to viewing angle effects.

To calculate an offset between two signatures for a satellite from two different systems we use linear interpolation to place the higher resolution signature (ROVOR) onto the lower resolution signature (Quad and SRO) x-axis grid. In doing so we can calculate an offset between Quad and ROVOR, and an offset between SRO and ROVOR. We can then calculate the average of the offset. Using this we can then calculate the average color index, again under the supposition that the offset is purely due to the color term. The results of this are shown below in Tab. 8. Based on the calculated color index of Galaxy-25 and Galaxy-28, assuming all of the offset is attributed to the color term, the color index is not consistent with the historical database of the GCPC. This implies that the viewing angle difference is a non-negligible contribution to the offset between the satellite signatures of Quad/SRO and ROVOR. We can also estimate the viewing angle difference contribution in magnitudes by using the historical average B-V index from GCPC from Tab. 3, using the following expression,

$$\text{offset} = \text{color term difference} + \text{viewing angle contribution}$$

$$\text{offset} = (T_2-T_1)*CI + \text{viewing angle contribution}$$

And taking the average gives,

$$\text{average}(\text{offset} = (T_2-T_1)*CI + \text{viewing angle contribution})$$

And noting that T_2-T_1 is a constant we have,

$$\text{average(offset)} = (T_2-T_1)*\text{average(CI)} + \text{average(viewing angle contribution)}$$

$$\text{average(viewing angle contribution)} = \text{average(offset)} - (T_2-T_1)*\text{average(CI)}$$

These results are shown below in Tab. 8, the average of the absolute values of the viewing angle contribution is not too large, of the order of 0.1 magnitude. Based on these calculations, the viewing angle contribution is about 1/3 of the offset and the color term contribution is about 2/3 of the offset.

Tab. 8. Calculation of Satellite Color Index and Viewing Angle Contribution

		Quad - ROVOR				SRO - ROVOR			
Satellite	average(B-V)$_{target}$ from Tab. 3 [mag]	average(Quad - ROVOR) Offset [mag]	T_{ROVOR}-T_{Quad} for (B-V) Index	average(B-V)$_{target}$ for Quad – ROVOR assuming offset is color term [mag]	Average Viewing Angle Contribution using Tab. 3 average(B-V)$_{target}$ Index [mag]	average(SRO - ROVOR) Offset [mag]	T_{ROVOR}-T_{SRO} for (B-V) Index	average(B-V)$_{target}$ for SRO – ROVOR assuming offset is color term [mag]	Average Viewing Angle Contribution using Tab. 3 average(B-V)$_{target}$ Index [mag]
Galaxy-19	N/A	0.27	0.29	0.93	N/A	0.21	0.20	1.05	N/A
Galaxy-25	0.97	0.13	0.29	0.45	-0.15	0.09	0.20	0.45	-0.10
Galaxy-28	0.66	0.25	0.29	0.86	0.06	0.21	0.20	1.05	0.08

Fig. 22, Fig. 23, and Fig. 24 below show the offset between ROVOR and JBO telescopes for Galaxy-19, Galaxy-25, and Galaxy-28, respectively. For Galaxy-19 the signatures show specular peaks with an overlap between the sites at -5 to -10 deg and at 20 deg LPA. The offset plot for Galaxy-19 shows a decrease around -5 deg and around 20 deg LPA, consistent with the color index becoming bluer (color term decreasing) due to a specular feature. For Galaxy-25 the signatures show specular peaks with an overlap between the sites at 0 deg and 20 deg LPA. The offset plot for Galaxy-25 shows a decrease around 5 deg LPA, consistent with the color index becoming bluer. While at 20 deg LPA the offset shows a small decrease but the surrounding data is increasing in general. For Galaxy-28 the signatures show specular peaks with an overlap between the sites at -5 to -10 deg and at ~ 20 deg LPA. The offset plot for Galaxy-28 shows a significant decrease in offset around -5 deg and there is a general decrease around 15 deg and a local decrease for Quad near 20 deg LPA. This trend of the offset decreasing near specular peaks provides additional evidence that a fraction of the offset is due to a color term.

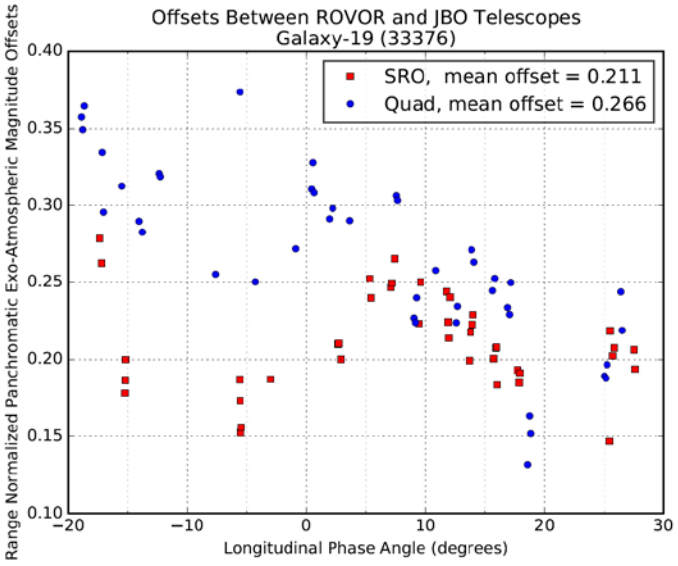

Fig. 22. Offset between ROVOR and JBO telescopes for Galaxy-19.

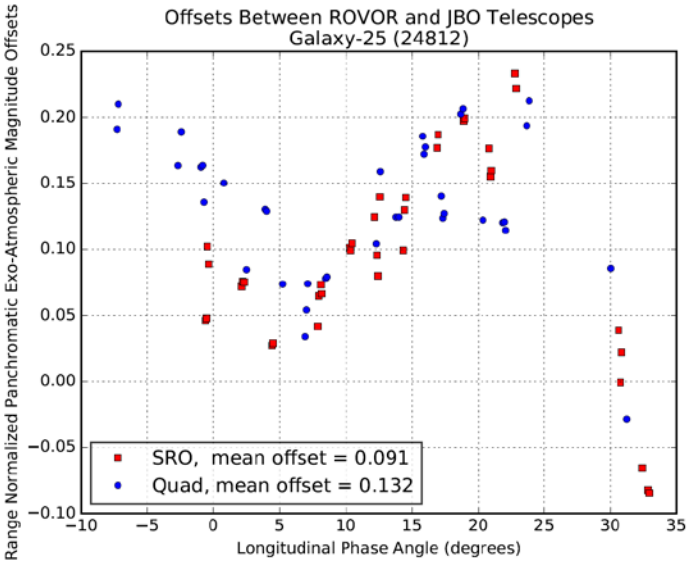

Fig. 23. Offset between ROVOR and JBO telescopes for Galaxy-25.

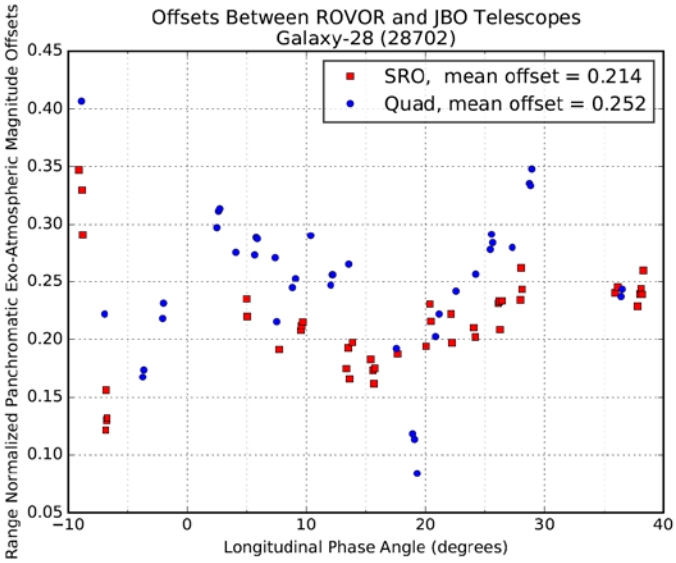

Fig. 24. Offset between ROVOR and JBO telescopes for Galaxy-28.

For two systems at the same site, viewing angle and atmosphere differences play no role and the offset is contributed purely to the color term. The difference in color coefficients between Quad and SRO is small, as is their offset. However, if two systems at the same site had a considerable difference in color coefficients, akin to that of Quad/SRO and ROVOR, such that the color term differences produced an offset larger than the error bars, then the offset between their signatures would be contributed solely to the color term. In this situation, the above process may be repeated to extract the color index of the satellite from two panchromatic systems at the same site. This offers an advantage over the traditional approach of in-band photometry to obtain the color indices, such as increased cadence. It also has the potential to perform observations with less than photometric conditions since clouds are gray bodies and will attenuate all wavelengths equally and similarly for both systems given close

proximity at the same site and near simultaneous observations of the target. There may also be disadvantages, such as an increase in photometric error due to the additional steps of calculating the color coefficient, this increases the error over a single step standard star calibration process of directly calculating the extinction coefficient and the zero point magnitude.

An important conclusion from the satellite signatures is that two panchromatic systems at two different sites can produce panchromatic magnitudes that are close to the Johnson-Cousins photometric system, but not exactly on it. With offsets of the order of ~0.2 mag between Quad/SRO and ROVOR, the color term and viewing angle of the satellite is important and cannot be ignored. For systems with a small color coefficient, a color term may be negligible, such that observations properly calibrated using the derived Open magnitudes should put the satellite observations on the Johnson-Cousins photometric system. This does not mean that the signatures from two geographically different sites will overlap even if calibrated on the Johnson-Cousins photometric system with a negligible color term due to the satellite target. The viewing angle differences appear to be real and are correct from the perspective of each observer. Even if the photometry is calibrated onto the Johnson-Cousins photometric system there may be differences in the photometry between two different geographic locations due to viewing angle differences. The contribution from the viewing angle differences warrants further investigation.

4.4 Verification of Derived Synthetic Open Magnitudes on the Johnson-Cousins Photometric System

Using the observations of the standard stars and the observation of SA114-750, we calculated an Open magnitude for each standard star for each system (Quad, SRO, and ROVOR) that is close to the Johnson-Cousins photometric system, except for a color term. These Open magnitudes were derived by using SA114-750 as the calibration star to put the observations of each standard star close to the Johnson-Cousins photometric system. From Pogson's equation,

$$m_1 - m_2 = -2.5*\log_{10}(F_1/F_2)$$

where m_1 is the magnitude of a standard star, and m_2 is the Open magnitude of the calibration star, SA114-750. Since SA114-750 has color indices near zero, we use the V magnitude from [10] as the Open magnitude. F_1 is the exo-atmospheric instrumental flux of a standard star and F_2 is the exo-atmospheric instrumental flux of SA114-750. F_1 and F_2 were empirically measured by each system, Quad, SRO, and ROVOR.

The empirically measured magnitude of each standard star using this technique is independent of the synthetically derived Open magnitude of each standard star. Once we include the empirically derived color term needed to put the measured magnitude completely onto the Johnson-Cousins system, we are then incorporating something that was derived using the synthetic Open magnitudes, since the color term was calculated using the synthetic Open magnitudes.

Tab. 9, Tab. 10, and Tab. 11 below show a comparison of the empirical Open magnitude and the synthetically derived Open magnitude for Quad, SRO, and ROVOR, respectively. For Quad, the empirically measured Open magnitude of the standard stars is quite close to the synthetic, with a difference for the standard stars of less than 0.02 mag or 2%. This is consistent with Quad having a color coefficient close to zero and implies that it is more or less on the Johnson-Cousins photometric system without a color term. After applying the empirically derived color term there is a difference for the standard stars of less than 0.06 mag (6%). The average of the absolute value of the difference of each star is 0.026 mag (2.6%). The difference is larger due to the uncertainty associated with the color coefficient for Quad, 0.037. For SRO the difference for the standard stars is less than 0.2 mag. Recall that SRO has a small but non-negligible color coefficient. After applying the empirically derived color term the difference is less

than 0.08 mag (8%), with an average of the absolute value of each star being 0.044 mag (4.4%). The uncertainty associated with the color coefficient for SRO is 0.050. For ROVOR the difference for the standard stars is as high as ~ 0.4 mag. This is consistent with ROVOR having a larger color coefficient. After applying the empirically derived color coefficient of ROVOR there is a difference of less than 0.06 mag (6%), with an average of the absolute value of each star being 0.037 mag (3.7%). The uncertainty associated with the color coefficient for ROVOR is 0.015. It is important to take into consideration the uncertainty associated with using SA114-750, which was the best calibration star available at the time but not an ideal one. For the deviation of color indices of SA114-750 from zero see Tab. 4. In addition, once the color coefficient is used to apply a color term to the empirically measured Open magnitude, there is an uncertainty associated with the color coefficient for each system that is included in the final empirically measured Open magnitude. In particular, for Quad, which has a color coefficient close to zero, the largest difference between the synthetic Open magnitude and empirically measured Open magnitude increases after including the color term, with the largest difference being consistent with the uncertainty associated with the color coefficient of Quad. With all this under consideration, these results provide evidence that the synthetically derived Open magnitudes are indeed on the Johnson-Cousins photometric system.

Tab. 9. Comparison of Synthetically Derived Open Magnitude and Empirical Open Magnitude for Quad

Quad							
Star	Derived Synthetic Open Magnitude	Empirically Measured Open Magnitude	Difference	B-V	Color Coefficient	Empirically Derived Color Term	Difference using Empirically Derived Color Term
SA109-71	11.561	11.544	0.017	0.326	-0.03	-0.010	0.027
SA109-381	11.741	11.743	-0.002	0.704	-0.03	-0.021	0.019
SA109-231	9.233	9.222	0.011	1.465	-0.03	-0.044	0.055
SA109-537	10.381	10.395	-0.014	0.609	-0.03	-0.018	0.004
average							0.026

Tab. 10. Comparison of Synthetically Derived Open Magnitude and Empirical Open Magnitude for SRO

SRO							
Star	Derived Synthetic Open Magnitude	Empirically Measured Open Magnitude	Difference	B-V	Color Coefficient	Empirically Derived Color Term	Difference using Empirically Derived Color Term
SA109-71	11.561	11.515	0.046	0.326	0.06	0.020	0.026
SA109-381	11.741	11.713	0.028	0.704	0.06	0.042	-0.014
SA109-231	9.233	9.068	0.165	1.465	0.06	0.088	0.077
SA109-537	10.381	10.286	0.095	0.609	0.06	0.037	0.058
average							0.044

Tab. 11. Comparison of Synthetically Derived Open Magnitude and Empirical Open Magnitude for ROVOR

ROVOR							
Star	Derived Synthetic Open Magnitude	Empirically Measured Open Magnitude	Difference	B-V	Color Coefficient	Empirically Derived Color Term	Difference using Empirically Derived Color Term
SA109-71	11.561	11.444	0.117	0.326	0.26	0.085	0.032
SA109-381	11.741	11.534	0.207	0.704	0.26	0.183	0.024
SA109-231	9.233	8.798	0.435	1.465	0.26	0.381	0.054
SA109-537	10.381	10.183	0.198	0.609	0.26	0.158	0.040
average							0.037

5. CONCLUSIONS

We derived synthetic Open magnitudes on the Johnson-Cousins photometric system via theoretical modeling. We produced a catalog of 289 standard stars with Open magnitudes for use by the community to calibrate panchromatic systems. To provide evidence that the synthetic Open magnitudes are on the Johnsons-Cousins photometric system, we compare our synthetic Open magnitude to the catalog magnitude of [10] for SA98-653, an A0V star. Its synthetic Open magnitude and the V band catalog magnitude are comparable, with a difference of 1.0%. Additional evidence that our synthetic Open magnitudes are on the Johnson-Cousins photometric system is demonstrated by comparing them to empirically measured Open magnitudes of four standard stars calibrated using SA114-750, a Vega-like star. After applying a color term we have shown that our synthetic Open magnitudes are on average within a few percent to 5% of the empirically measured Open magnitudes, i.e. on the order of the uncertainty associated with the empirical Open magnitudes. Our synthetic Open magnitudes of standard stars are used to calibrate satellite signatures from three different systems at two different geographic sites approximately onto the Johnson-Cousins photometric system via all-sky calibrations. This is an approximation due to a color term of the target satellite that is unknown. The offset between two systems at the same site is attributed to and consistent with a color term, while the offset between two systems at different geographical locations is attributed to a color term and viewing angle differences of the satellite. The average offset between satellite signatures at different geographic locations is up to ~0.3 mag, and from the average offsets of both Galaxy-25 and Galaxy-28 it was found that ~2/3 of the offset is due to a color term and ~1/3 of the offset is due to viewing angle differences. If a color index for a satellite were somehow known during the panchromatic observations, and a color term correction was applied to the satellite photometry, this would put satellite photometry from two systems at different locations on the Johnson-Cousins photometric system. Those final results would allow for multi-site, multi-sensor fusion of the photometry. However, signatures of the satellite may still have an offset due to viewing angle differences that are real and correct from the perspective of each observer. The color term of the satellite is a non-negligible factor that cannot be ignored to calibrate the photometry onto the standard system so that satellite photometry from different systems can be compared.

Without a satellite color index to calculate a color term, ideally the color coefficient of panchromatic systems needs to be characterized so that the size of the satellite color term can be estimated to determine the inaccuracies that may exist when comparing panchromatic data from different systems that are not quite on the Johnsons-Cousins photometric system. Two simplistic approaches present themselves in dealing with the unknown satellite color term

correction so that panchromatic data can be accurately compared between two systems. 1) Panchromatic satellite photometry from a system with a color coefficient of near zero would already be on the Johnson-Cousins photometric system without the need for a color term correction. Panchromatic satellite photometry collected with such a system could be compared with other panchromatic satellite photometry measurements that are on the Johnsons-Cousins photometric system. 2) Panchromatic satellite photometry from two identical systems with a color coefficient that is non-zero will not be on the Johnson-Cousins photometric system. However, the panchromatic satellite photometry will be comparable between the two systems, since their offset is the same amount for each system. The best approach to dealing with the satellite color term is a topic for future research and discussion.

6. FUTURE WORK

6.1 Tycho 2 Catalog

Future work should include applying the panchromatic calibration procedure outlined in this paper to the Tycho 2 catalog. The Tycho 2 catalog was analyzed by [15] in a similar fashion as the stars from [10]. They used Pickles Spectral Library and by fitting photometry to the spectra were able to provide spectral types for (~2.4 million) Tycho 2 stars. They also provide fitted UBVRI Johnson-Cousins photometry for these Tycho 2 stars. This provides the necessary ingredients to apply the same panchromatic calibration technique as done in this paper to the Tycho 2 catalog from [15]. This should result in calibrated panchromatic photometry on the Johnson-Cousins photometric system for ~1 - 2 million stars in the sky. This would create a catalog of stars with calibrated panchromatic magnitudes covering virtually the entire sky. This may allow in-frame panchromatic calibrations given a system has a sufficient FOV ~30 – 60 arc-minutes, in order to obtain a sufficient number of stars.

The fitted UBVRI photometry from the table of Tycho 2 stars from [15] would first need to be verified as being on the Johnson-Cousins photometric system, or close to it. A first step would be to take the fitted UBVRI photometry of the [10] stars from [15] which employed the same fitting process as applied to the Tycho 2 stars and compare this to the measured UBVRI photometry of [10]. This comparison between the fitted and measured UBVRI photometry would allow a determination of how close the fitting process is to the Johnson-Cousins system, and an estimate of the error that may be associated with it. This would need to be followed by a verification of the derived synthetic panchromatic magnitudes of the Tycho 2 stars in a similar fashion as was done in this paper for the [10] standard stars. The use of Tycho 2 stars (which are not standard stars) to perform calibrations would need to be assessed. The utility of a catalog of panchromatic magnitudes for ~1 - 2 million Tycho 2 stars in the sky for in-frame calibrations would provide a valuable asset to the SSA community.

6.2 Calculating Color Index of a Satellite using Two Panchromatic Systems at the Same Site

With the potential ability to obtain a color index of a satellite from two panchromatic systems at the same site, the opportunity presents itself to perform a study. Future work towards this end could be accomplished using three systems at the same site, two panchromatic with differing spectral responses and the third with the ability to collect Johnson-Cousins BVRI photometry. Observing the same satellite throughout the night would allow an investigation of the proposed technique. The two panchromatic systems would produce all combinations of color indices for a satellite (B-V, B-R, B-I, V-R, V-I, R-I) using the color coefficients from the standard star calibrations, since we have BVRI photometry of the standard stars from [10]. By equating the offset of the satellite signatures to the difference in color terms, the color index of the satellite would be obtained. In this fashion the color index as a function of LPA could be calculated. The third system that collected in-band photometry could then obtain color indices for the satellite in the traditional manner. The color indices between the panchromatic systems and that of the

color system could then be compared to test the validity of the proposed technique to extract color indices using two panchromatic systems at the same site, and characterize the color indices in their accuracy and precision as compared to the standard approach.

7. ACKNOWLEDGEMENTS

We thank AFRL/RY for the use of the facilities and telescope assets at John Bryan State Park Observatory. This research has made use of the VizieR catalogue access tool, CDS, Strasbourg, France. This research has made use of "Aladin sky atlas" developed at CDS, Strasbourg Observatory, France. This research has made use of the SIMBAD database, operated at CDS, Strasbourg, France.

REFERENCES

[1] H. L. Johnson and W. W. Morgan, "Fundamental Stellar Photometry for Standards of Spectral Type on the Revised System of the Yerkes Spectral Atlas," *The Astrophysical Journal,* vol. 117, pp. 313-352, 1953.

[2] H. L. Johnson, R. I. Mitchell, B. Iriarte and W. Z. Wisniewski, "UBVRIJKL Photometry of the Bright Stars," *Communications of the Lunar and Planetary Laboratory,* vol. 4, p. 99, 1966.

[3] M. S. Bessell, "Standard Photometric Systems," *Annual Review of Astronomy & Astrophysics,* vol. 43, pp. 293-336, 2005.

[4] G. E. Kron, H. S. White and S. C. B. Gascoigne, "Red and Infrared Magnitudes for 138 Stars Observed as Photometric Standards," *The Astrophysical Journal,* vol. 118, pp. 502-510, 1953.

[5] A. W. J. Cousins, "VRI Standards in the E Regions," *Memoirs of the Royal Astronomical Society,* vol. 81, pp. 25-36, 1976.

[6] A. U. Landolt, "UBVRI Photometric Standard Stars Around the Celestial Equator," *The Astronomical Journal,* vol. 88, pp. 439-460, 1983.

[7] A. U. Landolt, "UBV Photoelectric Sequences in the Celestial Equatorial Selected Areas," *The Astronomical Journal,* vol. 78, pp. 959-1021, 1973.

[8] B. D. Warner, A Practical Guide to Lightcurve Photometry and Analysis, New York: Springer, 2006.

[9] A. U. Landolt, "UBVRI Photometric Standard Stars in the Magnitude Range 11.5 < V < 16.0 Around the Celestial Equator," *The Astronomical Journal,* vol. 104, pp. 340-491, 1992.

[10] A. U. Landolt, "UBVRI Photometric Standard Stars Around the Celestial Equator: Updates and Additions," *The Astronomical Journal,* vol. 137, pp. 4186-4269, 2009.

[11] A. U. Landolt, "UBVRI Photometric Standard Stars Around the Sky at +50 deg Declination," *The Astronomical Journal,* vol. 146, p. 131, 2013.

[12] T. E. Payne, S. A. Gregory, D. J. Sanchez, L. G. Finkner, D. M. Payne, L. Kann, C. K. Davis and D. Werling, "Space Object Identification of Geosynchronous Satellites," in *AMOS Technical Conference*, 1999.

[13] T. E. Payne, S. A. Gregory, J. Tombasco, K. Luu and L. Durr, "Satellite Monitoring, Change Detection, and Characterization Using Non-Resolved Electro-Optical Data from a Small Aperture Telescope," in *AMOS*, 2007.

[14] P. B. Stetson, "Homogeneous Photometry for Star Clusters and Resolved Galaxies. II. Photometric Standard Stars," *Publications of the Astronomical Society of the Pacific,* vol. 112, pp. 925-931, 2000.

[15] A. Pickles and E. Depagne, "All-Sky Spectrally Matched UBVRI - ZY and u'g'r'i'z' Magnitudes for Stars in the Tycho2 Catalog," *Publications of the Astronomical Society of the Pacific,* vol. 122, pp. 1437-1464, 2010.

[16] A. J. Pickles, "A Stellar Spectral Flux Library: 1150-25000 Angstroms," *Publications of the Astronomical Society of the Pacific,* vol. 110, pp. 863-878, 1998.

[17] D. S. Birney, G. Gonzalez and D. Oesper, Observational Astronomy, Second ed., Cambridge: Cambridge University Press, 2006.

[18] A. N. Cox, Ed., Allen's Astrophysical Quantities, Fourth ed., New York: Springer-Verlag, 2000.

[19] H. Karttunen, P. Kroger, H. Oja, M. Poutanen and K. J. Donner, Eds., Fundamental Astronomy, Fourth Edition ed., Berlin: Springer-Verlag, 2003.

[20] A. U. Landolt, "UBVRI Photometric Standard Stars Around the Sky at -50 deg Declination," *The Astronomical Journal,* vol. 133, pp. 2502-2523, 2007.

[21] A. J. Burgasser, "SDSS J080531.84+481233.0: An Unresolved L Dwarf/T Dwarf Binary," *The Astronomical Journal,* vol. 134, pp. 1330-1336, 2007.

[22] I. S. McLean, Electronic Imaging in Astronomy: Detectors and Instrumentation, Second Edition ed., New York: Praxis Publishing, 2008.

[23] J. W. Moody, B. Boizelle, K. Bates, B. Little, T. McCombs, J. Nelson, C. Pace, R. L. I. Pearson, J. Harrison, P. J. Brown and J. Barnes, "Remote Observatory for Variable Object Research (ROVOR)," *Publications of the Astronomical Society of the Pacific,* vol. 124, pp. 956-962, 2012.

[24] G. H. Rieke, Measuring the Universe: A Multiwavelength Perspective, Cambridge: Cambridge University Press, 2012.

[25] B. Buchheim, "The Magnitude and Constancy of Second-Order Extinction at a Low-Altitude Observatory Site," in *The Society for Astronomical Sciences 24th Annual Symposium on Telescope Science*, 2005.

[26] J. S. Drilling and A. U. Landolt, "Spectral Classifications for Landolt's Celestial Equatorial Standard Stars," *The Astronomical Journal,* vol. 84, pp. 783-786, 1979.

8. APPENDIX

8.1 Standard Star Catalog of Open Magnitudes

Below in Tab. 12 we provide our catalog of Open magnitudes. Columns 1 to 9 contain information from [10]. Column 10 is the Open magnitude derived from this paper. Columns 11 and 12 are the proper motion of Right Ascension and Declination in units of mas yr^{-1}, respectively, again from [10]. And Column 13 is the spectral type from [15].

Tab. 12. Calibrated Open Magnitudes of Standard Stars

Star	α (J2000.0)	δ (J2000.0)	V	B-V	U-B	V-R	R-I	V-I	Open	μ_α	μ_δ	Spectral Type
	(h m s)	(d m s)								(mas yr^{-1})	(mas yr^{-1})	
(1)	(2)	(3)	(4)	(5)	(6)	(7)	(8)	(9)	(10)	(11)	(12)	(13)
TPhe I	00 30 04.593	-46 28 10.17	14.82	0.764	0.338	0.422	0.395	0.817	14.875	13.6	-8.5	G8V
TPhe A	00 30 09.594	-46 31 28.91	14.651	0.793	0.38	0.435	0.405	0.841	14.727	8.3	-2	wG5III
TPhe H	00 30 09.683	-46 27 24.30	14.942	0.74	0.225	0.425	0.425	0.851	14.983	11.2	-8.1	G8V
TPhe B	00 30 16.313	-46 27 58.57	12.334	0.405	0.156	0.262	0.271	0.535	12.397	1	-5.4	wF8V
TPhe D	00 30 18.342	-46 31 19.85	13.118	1.551	1.871	0.849	0.81	1.663	12.922	2.3	1.3	rK5III
TPhe J	00 30 23.020	-46 23 51.60	13.434	1.465	1.229	0.98	1.063	2.043	13.044	-16	-208	M2V
TPhe F	00 30 49.820	-46 33 24.07	12.475	0.853	0.534	0.492	0.437	0.929	12.531	80.6	-10.2	wG8III
HD 2892	00 32 12.153	+01 11 17.28	9.36	1.322	1.414	0.692	0.628	1.321	9.333	7.8	-1	wK4III
BD -15 115	00 38 20.261	-14 59 54.14	10.885	-0.199	-0.838	-0.095	-0.11	-0.204	10.577	7.1	1.4	B3III
92 312	00 53 16.533	+00 48 28.90	10.598	1.636	1.992	0.898	0.906	1.806	10.36	-0.3	-5.5	M2III
92 249	00 54 33.589	+00 41 05.39	14.325	0.699	0.24	0.399	0.37	0.77	14.374	10.4	-10.6	rG5V
92 250	00 54 37.154	+00 38 57.57	13.178	0.814	0.48	0.446	0.394	0.84	13.24	40.1	-8.1	K0V
92 252	00 54 47.255	+00 39 24.55	14.932	0.517	-0.14	0.326	0.332	0.666	14.977	-5.6	-18.2	rF8V
92 339	00 55 03.250	+00 44 11.00	15.579	0.449	-0.177	0.306	0.339	0.645	15.597	16	-10	wF8V
92 342	00 55 09.905	+00 43 12.88	11.615	0.435	-0.037	0.265	0.271	0.537	11.643	-1.9	-1.4	F5V
92 409	00 55 11.977	+00 55 57.53	10.627	1.138	1.136	0.734	0.625	1.361	10.545	-230.4	-127.6	K5V
92 410	00 55 14.254	+01 01 51.05	14.984	0.398	-0.134	0.239	0.242	0.484	15.03	4.1	-11.4	wF5V
92 412	00 55 15.666	+01 01 54.33	15.036	0.457	-0.152	0.285	0.304	0.589	15.079	5	-9.1	wF8V
92 263	00 55 39.384	+00 36 19.50	11.782	1.046	0.844	0.562	0.521	1.083	11.813	6.3	-2.3	K1III
92 425	00 55 58.180	+00 52 58.49	13.941	1.191	1.173	0.755	0.627	1.384	13.842	-25.5	-13.2	K5V
92 430	00 56 15.198	+00 53 18.20	14.44	0.567	-0.04	0.338	0.338	0.676	14.482	1.2	-8.3	rF8V
92 276	00 56 26.598	+00 41 50.72	12.036	0.629	0.067	0.368	0.357	0.726	12.075	3.5	-42	wG5V
92 282	00 56 46.817	+00 38 29.50	12.969	0.318	-0.038	0.201	0.221	0.422	13.006	22.1	-7.3	F02IV
92 288	00 57 17.005	+00 36 48.67	11.631	0.858	0.472	0.491	0.441	0.932	11.671	3.3	4.4	G5III
F 11A	01 04 27.970	+04 11 55.40	14.475	0.841	0.454	0.479	0.426	0.907	14.516	40	28	rK0V
F 11B	01 04 28.389	+04 11 25.09	13.784	0.747	0.234	0.437	0.412	0.849	13.821	17.1	2.4	G8V
93 407	01 54 37.126	+00 53 47.93	11.971	0.852	0.564	0.487	0.421	0.908	12.009	78.9	-31.9	rK0V
93 317	01 54 37.728	+00 43 00.57	11.546	0.488	-0.053	0.293	0.299	0.592	11.573	-9.3	-19.3	F6V
93 333	01 55 05.218	+00 45 42.57	12.009	0.833	0.436	0.469	0.422	0.892	12.056	19.7	-2.3	wG5III
93 424	01 55 26.364	+00 56 42.63	11.619	1.083	0.929	0.553	0.501	1.056	11.665	4.8	-2.8	K1III
G3 33	02 00 12.959	+13 03 07.01	12.298	1.802	1.306	1.355	1.752	3.103	11.231	-1092	-1772.9	M4V
PG0231+051E	02 33 28.872	+05 19 48.38	13.809	0.677	0.207	0.383	0.369	0.752	13.863	-6.5	-9.9	G0III
PG0231+051D	02 33 34.000	+05 19 30.90	14.031	1.077	1.026	0.671	0.584	1.252	13.977	50	-36	K4V
PG0231+051A	02 33 40.067	+05 17 40.68	12.768	0.711	0.271	0.405	0.388	0.794	12.808	-9	-46.7	rG5V
PG0231+051B	02 33 45.528	+05 17 33.30	14.732	1.437	1.279	0.951	0.991	1.933	14.391	15.1	-14.3	M1V
PG0231+051C	02 33 48.153	+05 20 26.36	13.707	0.678	0.078	0.396	0.385	0.783	13.729	-24.5	-30.8	G2V

F 24A	02 35 16.611	+03 43 16.78	13.822	0.525	0.034	0.314	0.319	0.635	13.847	7.8	-6.1	wF8V
F 24B	02 35 18.333	+03 42 40.37	13.546	0.668	0.188	0.382	0.367	0.749	13.583	18.8	-6.5	G2V
F 24C	02 35 26.318	+03 41 50.41	11.761	1.133	1.007	0.598	0.535	1.127	11.788	-12	-7.6	K2III
94 171	02 53 38.805	+00 17 18.60	12.659	0.817	0.304	0.48	0.483	0.964	12.694	18	10.3	rG5III
94 242	02 57 21.211	+00 18 38.67	11.725	0.303	0.11	0.176	0.184	0.362	11.773	-10.1	3.7	F0V
BD -2 524	02 57 39.679	-01 59 48.58	10.304	-0.111	-0.621	-0.048	-0.06	-0.108	10.038	4.8	-2.5	B5II
94 251	02 57 46.982	+00 16 02.72	11.204	1.219	1.281	0.659	0.586	1.245	11.181	24.9	-7.3	K3III
94 702	02 58 13.362	+01 10 54.30	11.597	1.416	1.617	0.757	0.675	1.431	11.51	-0.9	-3.4	K4III
95 301	03 52 41.167	+00 31 21.44	11.216	1.293	1.298	0.692	0.62	1.311	11.17	1.8	-10.6	rK3III
95 302	03 52 42.176	+00 31 17.71	11.694	0.825	0.447	0.471	0.42	0.891	11.74	39.2	-44.1	wG5III
95 96	03 52 54.194	+00 00 18.82	10.01	0.147	0.077	0.079	0.095	0.174	10.051	13.4	-2	A5V
95 317	03 53 44.183	+00 29 50.02	13.449	1.32	1.12	0.768	0.708	1.476	13.329	7.7	-11	rK4III
95 263	03 53 47.002	+00 26 40.82	12.679	1.5	1.559	0.801	0.711	1.513	12.565	2.9	-9.8	K5III
95 43	03 53 48.609	-00 03 01.74	10.803	0.51	-0.016	0.308	0.316	0.624	10.832	5.4	-12.7	wF8V
95 271	03 54 16.298	+00 18 52.20	13.669	1.287	0.916	0.734	0.717	1.453	13.572	7.2	-4	rK4III
95 328	03 54 19.470	+00 36 31.79	13.525	1.532	1.298	0.908	0.868	1.776	13.286	7.1	-3.2	M1III
95 60	03 54 49.540	-00 07 04.10	13.429	0.776	0.197	0.464	0.449	0.914	13.467	18	0	wG5III
95 218	03 54 49.948	+00 10 08.39	12.095	0.708	0.208	0.397	0.37	0.767	12.147	-6.3	-1.1	rG5V
95 132	03 54 51.685	+00 05 21.42	12.067	0.445	0.311	0.263	0.287	0.546	12.104	-2.7	-10.1	F5III
95 62	03 55 00.406	-00 02 54.09	13.538	1.355	1.181	0.742	0.685	1.428	13.45	0.8	-1.9	rK4III
95 142	03 55 09.394	+00 01 20.57	12.927	0.588	0.097	0.371	0.375	0.745	12.963	-7.7	-0.8	G2V
95 74	03 55 31.141	-00 09 13.57	11.531	1.126	0.686	0.6	0.567	1.165	11.544	0	2.1	K4V
95 231	03 55 38.828	+00 10 43.42	14.216	0.452	0.297	0.27	0.29	0.56	14.291	-0.2	-11.1	F8IV
95 236	03 56 13.342	+00 08 47.06	11.487	0.737	0.168	0.419	0.412	0.831	11.537	14.7	40.8	G8V
96 36	04 51 42.401	-00 10 09.47	10.589	0.247	0.118	0.133	0.137	0.271	10.642	-13.8	-0.7	A7III
96 737	04 52 35.366	+00 22 30.03	11.719	1.338	1.146	0.735	0.696	1.432	11.627	6.1	-11.7	wK4III
96 83	04 52 58.856	-00 14 41.18	11.719	0.181	0.205	0.092	0.096	0.189	11.765	-1.4	-1.5	A5III
96 235	04 53 18.870	-00 05 01.54	11.138	1.077	0.89	0.557	0.509	1.066	11.179	2.6	1.2	K1III
G97 42	05 28 00.150	+09 38 38.30	12.443	1.639	1.259	1.171	1.485	2.655	11.689	-196.84	-759.52	M3V
G102 22	05 42 09.273	+12 29 21.60	11.509	1.621	1.134	1.211	1.59	2.8	10.68	1988.5	-1571.7	M4V
GD 71C	05 52 12.777	+15 52 44.30	12.325	1.159	0.849	0.655	0.628	1.274	12.278	-2	-5.4	wK3III
GD 71E	05 52 20.510	+15 52 08.10	13.634	0.824	0.428	0.472	0.423	0.892	13.679	-4	-26	wG5III
GD 71B	05 52 21.530	+15 52 41.61	12.599	0.68	0.166	0.404	0.399	0.8	12.636	-7.7	-20	rG5V
GD 71D	05 52 24.788	+15 54 58.01	12.898	0.57	0.097	0.359	0.363	0.719	12.935	-1	-3	rG0V
GD 71A	05 52 33.562	+15 51 59.38	12.643	1.176	0.897	0.651	0.621	1.265	12.602	0.8	-4.6	wK3III
97 249	05 57 07.560	+00 01 11.50	11.735	0.647	0.101	0.369	0.354	0.725	11.783	15.2	1.2	G2V
97 351	05 57 37.294	+00 13 43.99	9.779	0.201	0.092	0.124	0.14	0.264	9.817	-0.2	-0.9	A7V
97 75	05 57 55.085	-00 09 28.55	11.483	1.872	2.1	1.047	0.952	1.999	11.177	3	-6	M3II
97 284	05 58 25.033	+00 05 13.57	10.787	1.364	1.089	0.774	0.726	1.5	10.68	-2.1	-4.9	K7V
98 556	06 51 29.537	-00 24 50.78	14.137	0.338	0.126	0.196	0.243	0.437	14.204	6.5	0	F5IV
98 563	06 51 31.543	-00 26 25.60	14.162	0.416	-0.19	0.294	0.317	0.61	14.176	0.9	3	F6V

98 978	06 51 33.730	-00 11 31.53	10.574	0.609	0.094	0.348	0.321	0.669	10.626	24.8	-29.7	G0IV
98 185	06 52 01.886	-00 27 21.57	10.537	0.202	0.114	0.11	0.122	0.231	10.588	0.5	0.6	A7V
98 193	06 52 03.381	-00 27 18.41	10.026	1.176	1.152	0.614	0.536	1.151	10.05	1.2	-11.2	rK2III
98 650	06 52 04.528	-00 19 38.29	12.271	0.157	0.11	0.08	0.086	0.166	12.323	3.9	-3.4	A5III
98 653	06 52 04.954	-00 18 18.26	9.538	-0.003	-0.102	0.01	0.009	0.017	9.528	0.6	-4.1	A0V
98 666	06 52 09.945	-00 23 32.01	12.732	0.164	-0.004	0.091	0.108	0.2	12.774	-13.1	3.1	A5III
98 670	06 52 11.514	-00 19 16.37	11.93	1.357	1.325	0.727	0.654	1.381	11.864	-15.3	-8.1	wK4III
98 671	06 52 11.830	-00 18 25.30	13.385	0.968	0.719	0.575	0.494	1.071	13.4	2.6	-35.1	K3V
98 682	06 52 16.504	-00 19 40.97	13.749	0.632	0.098	0.366	0.352	0.717	13.8	-9.3	-12.1	G2V
98 685	06 52 18.468	-00 20 19.51	11.954	0.463	0.096	0.29	0.28	0.57	12.009	-0.2	-2.7	rF6V
98 1112	06 52 34.895	-00 15 25.84	13.975	0.814	0.286	0.443	0.431	0.874	14.037	16.7	-28.2	wG5III
98 1119	06 52 36.710	-00 14 31.61	11.878	0.551	0.069	0.312	0.299	0.611	11.931	-5	-6.3	F8IV
98 724	06 52 37.225	-00 19 20.39	11.118	1.104	0.904	0.575	0.527	1.103	11.141	5.3	-5.4	wK2III
98 1122	06 52 37.558	-00 17 03.70	14.09	0.595	-0.297	0.376	0.442	0.816	14.102	0.5	-11.3	G2V
98 733	06 52 40.073	-00 17 14.67	12.238	1.285	1.087	0.698	0.65	1.347	12.162	-6.5	-4.9	K3III
Ru 149G	07 24 11.928	-00 31 58.11	12.829	0.541	0.033	0.322	0.322	0.645	12.867	3	-8.1	F8IV
Ru 149B	07 24 17.572	-00 33 06.18	12.642	0.662	0.151	0.374	0.354	0.728	12.688	-9.3	-13.6	G2V
Ru 149E	07 24 18.409	-00 31 18.58	13.718	0.522	-0.007	0.321	0.314	0.637	13.757	2.4	-5.9	F8IV
Ru 152E	07 29 54.256	-02 05 30.83	12.362	0.042	-0.086	0.03	0.034	0.065	12.347	3.6	-0.3	A0III
Ru 152A	07 30 00.483	-02 06 22.67	14.341	0.543	-0.085	0.325	0.329	0.654	14.393	-4.4	0.1	rF8V
Ru 152C	07 30 02.570	-02 05 39.30	12.222	0.573	-0.013	0.342	0.34	0.683	12.261	20	-36	rF8V
Ru 152D	07 30 06.076	-02 04 37.51	11.076	0.875	0.491	0.473	0.449	0.921	11.132	-2.1	-3.1	rG5III
99 6	07 53 33.338	-00 49 37.45	11.055	1.252	1.289	0.65	0.577	1.227	11.044	-5.1	-2.4	K3III
99 367	07 54 11.855	-00 25 35.18	11.152	1.005	0.832	0.531	0.477	1.007	11.206	-5.7	2.6	wK1III
99 408	07 55 13.012	-00 25 32.85	9.807	0.402	0.038	0.253	0.247	0.5	9.841	-10.8	-6.1	F5IV
99 447	07 56 06.686	-00 20 42.37	9.419	-0.068	-0.22	-0.031	-0.041	-0.073	9.372	-10.8	-5.1	B9III
100 241	08 52 34.049	-00 39 48.96	10.14	0.157	0.106	0.078	0.085	0.162	10.194	2.7	-2.6	A5III
100 162	08 53 14.418	-00 43 30.35	9.15	1.276	1.495	0.649	0.552	1.202	9.165	-10.7	-11.6	rK3III
100 280	08 53 35.477	-00 36 41.16	11.799	0.493	-0.001	0.295	0.291	0.588	11.827	9.8	-8.7	F6V
100 394	08 53 54.515	-00 32 22.08	11.384	1.317	1.457	0.705	0.636	1.341	11.343	-1.4	-1	wK4III
PG0918+029D	09 21 21.936	+02 47 28.28	12.272	1.044	0.821	0.575	0.535	1.108	12.291	-15.6	-10.1	wK2III
PG0918+029B	09 21 32.924	+02 47 59.08	13.963	0.765	0.366	0.417	0.37	0.787	14.03	-13.7	-24.4	G8V
PG0918+029A	09 21 35.107	+02 46 19.43	14.49	0.536	-0.032	0.325	0.336	0.661	14.539	-7.1	-7.5	rF8V
PG0918+029C	09 21 42.306	+02 46 37.07	13.537	0.631	0.087	0.367	0.357	0.722	13.585	-13.2	9.3	G2V
BD -12 2918	09 31 19.370	-13 29 19.30	10.067	1.501	1.166	1.067	1.318	2.385	9.512	743.44	53.53	M3V
PG0942-029D	09 45 08.637	-03 05 54.45	13.683	0.576	0.064	0.341	0.329	0.668	13.727	-0.9	11.4	rF8V
PG0942-029A	09 45 09.900	-03 10 14.20	14.738	0.888	0.552	0.563	0.474	1.035	14.738	-12	6	K2V
PG0942-029B	09 45 11.574	-03 06 58.11	14.105	0.573	0.014	0.353	0.341	0.693	14.136	0.9	1.6	rF8V
PG0942-029C	09 45 14.386	-03 06 40.28	14.95	0.803	0.338	0.488	0.395	0.884	14.99	-14	-1.8	wG5III
101 315	09 54 51.298	-00 27 31.09	11.249	1.153	1.056	0.612	0.559	1.172	11.253	-0.9	-0.6	K2III
101 316	09 54 52.034	-00 18 34.51	11.552	0.493	0.032	0.293	0.291	0.584	11.605	3	-10.3	rF6V

101 320	09 55 32.924	-00 22 32.72	13.823	1.052	0.69	0.581	0.561	1.141	13.827	-6	-10	wK2III
101 404	09 55 40.673	-00 18 22.23	13.459	0.996	0.697	0.53	0.5	1.029	13.505	8.3	14.9	wK1III
101 324	09 55 56.650	-00 23 15.10	9.737	1.161	1.145	0.591	0.519	1.109	9.767	6.3	1.6	rK1III
101 326	09 56 08.101	-00 27 10.94	14.923	0.729	0.227	0.406	0.375	0.78	14.969	-5.6	-2.9	rG5V
101 327	09 56 08.860	-00 25 53.50	13.441	1.155	1.139	0.717	0.574	1.29	13.398	2	-38	K5V
101 413	09 56 14.009	-00 11 54.86	12.583	0.983	0.716	0.529	0.497	1.025	12.63	-13.5	7.5	wK1III
101 330	09 56 20.587	-00 27 22.12	13.723	0.577	-0.026	0.346	0.338	0.684	13.76	-13.8	-1.8	rF8V
101 281	09 57 05.020	-00 31 43.20	11.576	0.812	0.415	0.453	0.412	0.864	11.638	4.9	-3.6	wG5III
101 431	09 57 37.322	-00 17 53.28	13.684	1.246	1.144	0.808	0.708	1.517	13.553	4.7	-12.3	K7V
101 207	09 57 52.495	-00 47 36.17	12.421	0.513	-0.08	0.32	0.323	0.645	12.44	-4.8	5.4	wF8V
101 363	09 58 18.722	-00 25 36.51	9.874	0.26	0.132	0.146	0.151	0.297	9.943	1.2	-5.5	F0III
GD 108A	10 00 39.585	-07 33 25.10	13.881	0.789	0.316	0.458	0.449	0.909	13.924	-18.1	-4.8	wG5III
GD 108B	10 00 42.665	-07 31 07.90	15.056	0.839	0.364	0.463	0.466	0.924	15.095	-2.6	-10.6	wG5III
GD 108C	10 00 55.223	-07 30 29.59	13.819	0.786	0.345	0.435	0.393	0.825	13.889	1.5	-12.3	K0V
GD 108D	10 00 55.916	-07 34 51.83	14.235	0.641	0.078	0.372	0.357	0.731	14.279	-5.3	-6	G2V
BD +1 2447	10 28 55.551	+00 50 27.56	9.65	1.501	1.238	1.033	1.225	2.261	9.187	-602.7	-736.5	M3V
G44 27	10 36 01.210	+05 07 12.80	12.636	1.586	1.088	1.185	1.526	2.714	11.873	-661	128	M4V
PG1047+003A	10 50 05.653	-00 01 11.25	13.512	0.688	0.168	0.422	0.418	0.84	13.524	-12.8	-10.8	G0III
PG1047+003B	10 50 07.915	-00 02 04.36	14.751	0.679	0.172	0.391	0.371	0.764	14.804	-21.8	1.6	rG5V
PG1047+003C	10 50 13.682	-00 00 32.35	12.453	0.607	-0.019	0.378	0.358	0.737	12.483	-34.5	17.6	wG5V
G44 40	10 50 52.010	+06 48 29.30	11.675	1.644	1.213	1.216	1.568	2.786	10.855	-845	-815	M4V
102 1081	10 57 04.045	-00 13 12.87	9.903	0.664	0.258	0.366	0.332	0.697	9.974	4.1	-46.3	G2IV
G163 51B	11 07 32.846	-05 12 37.29	11.292	0.623	0.119	0.355	0.336	0.692	11.344	-63.3	3.2	rG0V
G163 51C	11 07 33.782	-05 14 20.26	12.672	0.431	-0.009	0.267	0.272	0.54	12.707	-13.1	4.7	F5III
G163 51D	11 07 34.915	-05 15 00.50	13.862	0.844	0.202	0.478	0.466	0.945	13.906	-11.7	-19.6	rG5III
G163 51A	11 07 37.196	-05 12 23.31	12.504	0.666	0.06	0.382	0.371	0.753	12.54	-45.1	-13.6	G2V
G163 51	11 08 06.539	-05 13 47.19	12.559	1.499	1.195	1.08	1.355	2.434	11.969	-55.8	-462.4	M3V
BD +5 2468	11 15 30.897	+04 57 23.52	9.352	-0.114	-0.543	-0.035	-0.052	-0.089	9.17	-36.2	9.6	B57V
HD 100340	11 32 49.941	+05 16 36.23	10.115	-0.234	-0.975	-0.104	-0.135	-0.238	9.668	2.9	11.9	B1V
BD +5 2529	11 41 49.593	+05 08 26.54	9.585	1.233	1.194	0.783	0.667	1.452	9.447	225.5	-469.3	K5V
G10 50	11 47 44.390	+00 48 16.40	11.153	1.752	1.318	1.294	1.673	2.969	10.19	595.1	-1222.5	M4V
103 302	11 56 06.021	-00 47 54.36	9.859	0.37	-0.057	0.23	0.236	0.465	9.897	-48.2	12.2	F2V
103 626	11 56 46.156	-00 23 14.71	11.836	0.413	-0.057	0.262	0.274	0.535	11.863	16.7	-8.6	F5V
103 526	11 56 54.182	-00 30 13.47	10.89	1.09	0.936	0.56	0.501	1.056	10.937	-15.3	13.1	wK2III
104 306	12 41 03.619	-00 37 13.83	9.37	1.592	1.666	0.832	0.762	1.591	9.216	5.6	-34.3	rK5III
104 428	12 41 41.284	-00 26 26.13	12.63	0.985	0.748	0.534	0.497	1.032	12.673	-5.4	-0.1	wK1III
104 430	12 41 50.259	-00 25 52.44	13.858	0.652	0.131	0.364	0.363	0.727	13.908	-8.7	-7.6	G2V
104 334	12 42 20.425	-00 40 28.35	13.484	0.518	-0.067	0.323	0.331	0.653	13.5	-20.5	-6.6	wF8V
104 336	12 42 24.640	-00 39 58.00	14.404	0.83	0.495	0.461	0.403	0.865	14.463	0	-4	wG5III
104 455	12 42 52.116	-00 24 17.43	15.105	0.581	-0.024	0.36	0.357	0.716	15.147	-9	-3.3	wG5V
104 461	12 43 06.031	-00 32 18.01	9.705	0.476	-0.035	0.288	0.289	0.579	9.736	-13.4	1.5	F6V

104 350	12 43 14.204	-00 33 20.54	13.634	0.673	0.165	0.383	0.353	0.736	13.675	0	-11.8	G2V
104 490	12 44 33.454	-00 25 51.78	12.572	0.535	0.048	0.318	0.312	0.63	12.615	1.5	-2.3	F8IV
104 598	12 45 16.779	-00 16 40.47	11.478	1.108	1.051	0.667	0.545	1.214	11.443	-136.1	-79.8	K4V
PG1323-086C	13 25 50.222	-08 48 38.94	14.003	0.707	0.245	0.395	0.363	0.759	14.058	-8.8	-16.4	rG5V
PG1323-086B	13 25 50.651	-08 50 55.10	13.406	0.761	0.265	0.426	0.407	0.833	13.454	8	-25.9	G8V
PG1323-086D	13 26 05.252	-08 50 36.19	12.08	0.587	0.005	0.346	0.335	0.684	12.118	-9.7	-10.3	rF8V
G14 55	13 28 21.082	-02 21 37.07	11.336	1.491	1.157	1.078	1.388	2.462	10.728	156.7	-492.5	M3V
105 505	13 35 24.773	-00 23 20.74	10.27	1.422	1.218	0.91	0.861	1.771	9.998	36.6	187.5	M0V
105 437	13 37 16.748	-00 37 56.33	12.535	0.248	0.067	0.136	0.143	0.279	12.611	-15.7	-10.8	F0III
BD +2 2711	13 42 19.004	+01 30 18.68	10.369	-0.163	-0.699	-0.072	-0.095	-0.168	10.057	-5.9	1.1	B3III
32376437	13 42 23.215	+01 30 25.71	10.584	0.499	0.005	0.304	0.301	0.606	10.619	-8.1	-2.7	wF8V
PG1407-013B	14 10 24.181	-01 27 16.52	12.471	0.97	0.665	0.537	0.505	1.037	12.485	-17.7	8.8	K2V
PG1407-013C	14 10 28.013	-01 25 03.05	12.462	0.805	0.298	0.464	0.448	0.914	12.502	-0.6	-23.8	wG5III
PG1407-013D	14 10 34.083	-01 27 14.00	14.872	0.891	0.42	0.496	0.472	0.967	14.904	-12	8.8	rG5III
PG1407-013E	14 10 35.721	-01 26 31.42	15.182	0.883	0.6	0.496	0.417	0.915	15.228	-17.3	5	G5III
106 700	14 40 50.944	-00 23 36.82	9.786	1.364	1.58	0.73	0.643	1.374	9.722	-17.1	3.8	wK4III
106 575	14 41 38.499	-00 26 01.82	9.341	1.306	1.485	0.676	0.587	1.268	9.319	-30.9	-7.8	rK3III
106 485	14 44 14.083	-00 37 06.69	9.477	0.378	-0.052	0.233	0.236	0.468	9.514	-6.3	13	F2V
PG1525-071A	15 28 13.416	-07 16 01.03	13.506	0.773	0.282	0.437	0.421	0.862	13.541	-11.6	-19.2	G8V
PG1525-071B	15 28 14.390	-07 16 13.20	16.392	0.729	0.141	0.45	0.387	0.906	16.424	-10	4	K0V
PG1525-071C	15 28 16.502	-07 14 30.36	13.519	1.116	1.073	0.593	0.509	1.096	13.551	-13.7	-10.9	rK1III
107 544	15 36 48.097	-00 15 07.07	9.036	0.399	0.156	0.232	0.227	0.458	9.097	0	26	F2III
107 970	15 37 25.830	+00 18 33.82	10.939	1.596	1.75	1.142	1.435	2.574	10.285	-6.1	-2.4	M4V
107 568	15 37 52.713	-00 17 17.51	13.054	1.149	0.862	0.625	0.595	1.217	13.041	-12.8	-11.1	wK3III
107 1006	15 38 33.353	+00 14 19.11	11.713	0.766	0.278	0.442	0.42	0.863	11.745	20.8	-24.7	G8V
107 347	15 38 35.770	-00 35 57.69	9.446	1.294	1.302	0.712	0.652	1.365	9.391	-23.3	-21.9	wK4III
107 456	15 38 42.735	-00 19 47.02	12.919	0.921	0.589	0.537	0.478	1.015	12.938	-31.2	8.7	K2V
107 351	15 38 45.760	-00 32 06.30	12.342	0.562	-0.005	0.351	0.358	0.708	12.368	-10.8	-5.1	rF8V
107 592	15 38 50.382	-00 17 09.17	11.847	1.318	1.38	0.709	0.647	1.357	11.797	-3.3	0.4	wK4III
107 599	15 39 09.457	-00 14 28.74	14.675	0.698	0.243	0.433	0.438	0.869	14.675	-9.2	-7.5	G0III
107 602	15 39 18.878	-00 15 29.94	12.116	0.991	0.585	0.545	0.531	1.074	12.139	-13.5	-9.1	wK1III
107 626	15 40 05.349	-00 17 28.95	13.468	1	0.728	0.6	0.527	1.126	13.465	25.2	-7.2	K1III
107 627	15 40 07.462	-00 17 22.68	13.349	0.779	0.226	0.465	0.454	0.918	13.385	2.7	-10.6	wG5III
107 484	15 40 16.818	-00 21 14.93	11.311	1.24	1.298	0.664	0.577	1.24	11.289	2.9	-12.7	K3III
BD -12 4523	16 30 18.059	-12 39 45.34	10.072	1.566	1.195	1.155	1.499	2.651	9.324	-95.9	-1184.9	M3V
HD 149382	16 34 23.333	-04 00 52.02	8.943	-0.282	-1.143	-0.127	-0.135	-0.262	8.482	-7.2	-4.6	B12III
108 1332	16 35 21.401	-00 04 05.32	9.208	0.38	0.083	0.225	0.225	0.449	9.254	-0.2	7.3	F2V
PG1633+099A	16 35 25.984	+09 47 53.19	15.259	0.871	0.305	0.506	0.506	1.011	15.271	5.9	-9.8	rG5III
PG1633+099B	16 35 33.304	+09 46 20.71	12.968	1.081	1.017	0.589	0.503	1.09	13.002	8	-8.9	rK1III
PG1633+099F	16 35 36.713	+09 49 40.34	13.768	0.878	0.254	0.523	0.522	1.035	13.765	-3.7	-12.4	rG5III
PG1633+099C	16 35 37.275	+09 46 15.80	13.224	1.144	1.146	0.612	0.524	1.133	13.243	-1.2	-8.7	K2III

PG1633+099D	16 35 40.089	+09 46 41.57	13.689	0.535	-0.021	0.324	0.323	0.649	13.707	-4.3	-5.4	wF8V
PG1633+099E	16 35 45.084	+09 49 24.53	13.113	0.841	0.337	0.484	0.471	0.953	13.152	-4.6	-5.1	rG5III
108 475	16 37 00.595	-00 34 39.17	11.307	1.38	1.463	0.743	0.664	1.408	11.228	-0.9	-2.3	rK4III
108 1491	16 37 13.934	-00 02 41.91	9.059	0.964	0.616	0.522	0.498	1.02	9.085	3.5	-18.1	K2V
108 551	16 37 47.788	-00 33 05.16	10.702	0.18	0.182	0.1	0.109	0.209	10.77	5.1	5.5	F0II
Wolf 629	16 55 25.223	-08 19 21.30	11.759	1.676	1.256	1.185	1.525	2.715	10.996	-816.9	-898.3	M4V
PG1657+078B	16 59 31.979	+07 42 07.34	14.724	0.697	0.039	0.417	0.42	0.838	14.739	-5	-1.5	G0III
PG1657+078C	16 59 35.270	+07 42 26.51	15.225	0.837	0.382	0.504	0.442	0.965	15.234	-11	-3.8	wG5III
BD -4 4226	17 05 13.783	-05 05 39.21	10.071	1.415	1.085	0.97	1.141	2.113	9.644	-915.3	-1130.4	M2V
109 71	17 44 06.792	-00 24 58.01	11.49	0.326	0.154	0.187	0.223	0.409	11.561	-0.6	-1.9	F2II
109 381	17 44 12.269	-00 20 32.80	11.731	0.704	0.222	0.427	0.435	0.862	11.741	-1.8	4.4	rG5V
109 231	17 45 19.964	-00 25 51.60	9.333	1.465	1.591	0.787	0.705	1.494	9.233	1.9	-14.3	K5III
109 537	17 45 42.448	-00 21 35.43	10.353	0.609	0.226	0.376	0.393	0.769	10.381	0.8	-1.2	G2V
110 232	18 40 52.340	+00 01 54.78	12.516	0.729	0.147	0.439	0.45	0.889	12.538	-11	-26.1	G8V
110 233	18 40 52.709	+00 00 50.85	12.771	1.281	0.812	0.773	0.818	1.593	12.617	-4.1	3.5	K7V
110 355	18 42 18.933	+00 08 24.22	11.944	1.023	0.504	0.652	0.727	1.378	11.846	-2.3	-3.6	K4V
110 361	18 42 45.010	+00 08 04.70	12.425	0.632	0.035	0.361	0.348	0.709	12.473	1.5	-5.6	wG5V
110 266	18 42 48.798	+00 05 06.44	12.018	0.889	0.411	0.538	0.577	1.111	12.001	0.5	4.5	K2V
110 364	18 42 52.785	+00 07 54.89	13.615	1.133	1.095	0.697	0.585	1.281	13.541	5.6	-10.4	K4V
110 497	18 43 02.506	+00 30 56.79	14.196	1.052	0.38	0.606	0.597	1.203	14.188	-1.5	-7.8	K4V
110 499	18 43 07.663	+00 28 01.47	11.737	0.987	0.639	0.6	0.674	1.273	11.683	2.6	0.2	wK2III
110 503	18 43 11.696	+00 29 42.95	11.773	0.671	0.506	0.373	0.436	0.808	11.819	5	-6	rG5V
110 441	18 43 33.607	+00 19 40.72	11.122	0.556	0.108	0.325	0.335	0.66	11.172	2.7	-14.3	wG0V
110 450	18 43 51.474	+00 22 58.46	11.583	0.946	0.683	0.549	0.626	1.175	11.568	-0.8	-10.9	K3V
111 773	19 37 15.832	+00 10 58.24	8.965	0.209	-0.209	0.121	0.145	0.265	8.982	7.8	2.1	A5V
111 1925	19 37 28.639	+00 25 02.74	12.387	0.396	0.264	0.226	0.256	0.483	12.436	2.3	-4.2	F5IV
111 1965	19 37 41.557	+00 26 50.94	11.419	1.71	1.865	0.951	0.877	1.83	11.151	1.2	5.8	M2III
111 1969	19 37 43.288	+00 25 48.55	10.382	1.959	2.306	1.177	1.222	2.4	9.781	4.8	0.7	M3II
111 2039	19 38 04.578	+00 32 12.54	12.395	1.369	1.237	0.739	0.689	1.43	12.308	-0.2	-12.7	rK4III
111 2088	19 38 21.254	+00 31 00.26	13.193	1.61	1.678	0.888	0.818	1.708	12.999	-4.2	-5.1	M1III
111 2093	19 38 23.462	+00 31 25.44	12.538	0.637	0.283	0.37	0.397	0.766	12.572	1.7	-3.7	G2V
112 595	20 41 18.463	+00 16 28.06	11.352	1.601	1.991	0.898	0.903	1.801	11.117	-0.9	-6.1	M2III
112 704	20 42 02.066	+00 19 08.22	11.452	1.536	1.742	0.822	0.746	1.57	11.311	-3.9	0.4	rK5III
112 223	20 42 14.583	+00 08 59.70	11.424	0.454	0.016	0.273	0.274	0.547	11.468	5.3	-10.4	F6V
112 250	20 42 26.386	+00 07 42.50	12.095	0.532	-0.025	0.317	0.323	0.639	12.118	1.4	-9.1	wF8V
112 275	20 42 35.424	+00 07 20.22	9.905	1.21	1.294	0.648	0.569	1.217	9.898	-0.8	-11.1	K3III
112 805	20 42 46.753	+00 16 08.08	12.086	0.151	0.158	0.064	0.075	0.139	12.141	8.9	11.6	A5V
112 822	20 42 54.915	+00 15 01.90	11.548	1.03	0.883	0.558	0.502	1.06	11.588	-2.6	-12.7	K1III
Mark A4	20 43 53.555	-10 45 05.17	14.767	0.795	0.176	0.471	0.475	0.952	14.79	1.5	-6.3	wG5III
Mark A2	20 43 54.998	-10 45 31.29	14.54	0.666	0.096	0.379	0.371	0.751	14.577	3.8	-1.6	G2V
Mark A1	20 43 58.451	-10 47 12.27	15.911	0.609	-0.014	0.367	0.373	0.74	15.952	-9.6	-2	G2V

Mark A3	20 44 03.820	-10 45 37.90	14.818	0.938	0.651	0.587	0.51	1.098	14.816	4	-24	K3V
Wolf 918	21 09 17.431	-13 18 09.01	10.869	1.493	1.139	0.978	1.083	2.064	10.468	721	-1992.3	M2V
G26 7A	21 31 06.807	-09 46 35.55	13.047	0.725	0.279	0.405	0.371	0.776	13.094	4	-21.9	rG5V
G26 7	21 31 18.637	-09 47 26.44	12.006	1.664	1.231	1.298	1.669	2.968	11.042	1209.7	-60.8	M4V
G26 7C	21 31 23.333	-09 50 46.60	12.468	0.624	0.093	0.354	0.34	0.695	12.519	46.6	-11.6	rG0V
G26 7B	21 31 26.454	-09 47 23.47	13.454	0.562	0.027	0.323	0.327	0.652	13.509	14.5	-25.4	rF8V
113 221	21 40 36.542	+00 21 03.31	12.071	1.031	0.874	0.55	0.49	1.041	12.122	-2.7	-2.9	K1III
113 337	21 40 49.456	+00 27 58.01	14.225	0.519	-0.025	0.351	0.331	0.682	14.256	-0.9	2.6	rF8V
113 339	21 40 55.675	+00 27 58.07	12.25	0.568	-0.034	0.34	0.347	0.687	12.288	2.6	-2.8	rF8V
113 342	21 40 59.843	+00 27 36.65	10.878	1.015	0.696	0.537	0.513	1.05	10.914	21.6	-2	wK1III
113 466	21 41 27.386	+00 40 15.56	10.003	0.453	0.003	0.279	0.283	0.564	10.04	20	7.4	F6V
113 259	21 41 44.849	+00 17 40.05	11.744	1.199	1.22	0.621	0.544	1.167	11.76	-7.7	-0.8	rK2III
113 260	21 41 48.071	+00 23 52.81	12.406	0.514	0.069	0.308	0.298	0.606	12.448	-8.4	-6.9	rF6V
113 475	21 41 51.293	+00 39 20.78	10.304	1.058	0.841	0.568	0.528	1.097	10.327	11.3	-15.4	K1III
113 492	21 42 27.808	+00 38 21.96	12.174	0.553	0.005	0.342	0.341	0.684	12.211	10.8	-8.8	rF8V
113 493	21 42 28.579	+00 38 11.53	11.767	0.786	0.392	0.43	0.393	0.824	11.818	22.5	4.1	G8V
113 495	21 42 29.737	+00 38 07.96	12.437	0.947	0.53	0.512	0.497	1.01	12.47	-10.8	0.7	K2V
113 163	21 42 35.438	+00 16 45.54	14.54	0.658	0.106	0.38	0.355	0.735	14.581	-2.4	-11	G2V
113 177	21 42 56.538	+00 14 43.80	13.56	0.789	0.318	0.456	0.436	0.89	13.61	13.5	-12	wG5III
113 182	21 43 08.336	+00 14 49.98	14.37	0.659	0.065	0.402	0.422	0.824	14.393	2.3	-0.2	G0III
113 191	21 43 33.561	+00 15 54.39	12.337	0.799	0.223	0.471	0.466	0.937	12.366	-16.7	-8.4	wG5III
113 195	21 43 40.819	+00 17 21.83	13.692	0.73	0.201	0.418	0.413	0.832	13.741	-1.5	-7.5	G8V
G93 48D	21 52 10.158	+02 21 25.52	13.664	0.636	0.12	0.368	0.362	0.724	13.705	-13.5	-11.8	wG5V
G93 48C	21 52 13.860	+02 21 52.90	12.664	1.32	1.26	0.852	0.759	1.61	12.473	104	-28	K7V
G93 48A	21 52 17.450	+02 23 14.20	12.856	0.715	0.278	0.403	0.365	0.772	12.904	40	-2	rG5V
G93 48B	21 52 18.349	+02 23 10.40	12.416	0.719	0.194	0.405	0.383	0.791	12.458	-12.6	-21.7	rG5V
PG2213-006F	22 16 12.898	-00 17 55.86	12.644	0.678	0.171	0.395	0.384	0.781	12.684	-7.2	-3.1	G0III
PG2213-006C	22 16 17.674	-00 22 14.30	15.108	0.726	0.175	0.425	0.432	0.853	15.118	4.5	-3.7	G0III
PG2213-006B	22 16 21.757	-00 21 48.50	12.71	0.753	0.291	0.427	0.404	0.831	12.758	21.5	-3.5	G8V
PG2213-006A	22 16 23.206	-00 21 26.98	14.18	0.665	0.094	0.407	0.408	0.817	14.203	18.5	-7.7	G0III
G156 31	22 38 33.592	-15 17 59.44	12.361	1.993	1.408	1.648	2.042	3.684	10.892	2310.5	2291.7	M6V
114 531	22 40 36.756	+00 51 55.46	12.095	0.733	0.175	0.421	0.404	0.824	12.122	-25.5	-16.3	rG5V
114 637	22 40 42.570	+01 03 10.62	12.07	0.801	0.307	0.456	0.415	0.872	12.116	0	0.8	K0V
114 654	22 41 26.140	+01 10 10.69	11.833	0.656	0.178	0.368	0.341	0.711	11.879	30	-10.8	wG5V
114 548	22 41 36.833	+00 59 05.80	11.599	1.362	1.568	0.738	0.651	1.387	11.526	-0.5	-6.4	wK4III
114 755	22 42 07.584	+01 16 48.99	10.909	0.57	-0.063	0.313	0.31	0.622	10.96	-71.3	-40.9	F8V
114 670	22 42 09.288	+01 10 16.80	11.101	1.206	1.223	0.645	0.561	1.208	11.091	-9.8	-13.9	rK2III
114 176	22 43 10.181	+00 21 15.57	9.239	1.485	1.853	0.8	0.717	1.521	9.121	-4.7	-6.2	K5III
G156 57	22 53 16.728	-14 15 49.32	10.192	1.557	1.179	1.179	1.543	2.73	9.419	951	-676	M4V
GD 246A	23 12 17.442	+10 46 12.87	12.962	0.463	-0.047	0.288	0.296	0.584	12.99	-4.3	-8.4	F6V
GD 246B	23 12 28.998	+10 47 11.37	14.368	0.919	0.693	0.512	0.431	0.944	14.425	0.9	-14.9	G8III

GD 246C	23 12 30.920	+10 49 13.96	13.637	0.879	0.54	0.484	0.448	0.933	13.681	-3.4	-0.4	G5III
PG2336+004B	23 38 38.287	+00 42 46.40	12.429	0.517	-0.048	0.313	0.317	0.627	12.456	10.4	-1.1	wF8V
115 486	23 41 32.988	+01 16 44.80	12.482	0.493	-0.049	0.298	0.308	0.607	12.518	0.2	-7	wF8V
115 420	23 42 36.481	+01 05 58.82	11.16	0.467	-0.019	0.288	0.293	0.581	11.19	-5.7	-6.7	F6V
115 271	23 42 41.825	+00 45 13.14	9.693	0.612	0.109	0.354	0.349	0.702	9.741	62	28.2	rG0V
115 516	23 44 15.370	+01 14 12.70	10.431	1.028	0.76	0.564	0.534	1.099	10.454	30.2	-21.4	K1III
BD +1 4774	23 49 12.526	+02 24 04.42	8.993	1.434	1.105	0.964	1.081	2.047	8.605	993.7	-966.7	M2V